Design, synthesis and in vitro kinetic study of tranexamic acid prodrugs for the treatment of bleeding conditions

Rafik Karaman · Hiba Ghareeb · Khuloud Kamal Dajani · Laura Scrano · Hussein Hallak · Saleh Abu-Lafi · Gennaro Mecca · Sabino A. Bufo

Abstract Based on density functional theory (DFT) calculations for the acid-catalyzed hydrolysis of several maleamic acid amide derivatives four tranexamic acid prodrugs were designed. The DFT results on the acid catalyzed hydrolysis revealed that the reaction rate-limiting step is determined on the nature of the amine leaving group. When the amine leaving group was a primary amine or tranexamic acid moiety, the tetrahedral intermediate collapse was the rate-limiting step, whereas in the cases by which the amine leaving group was aciclovir or cefuroxime the rate-limiting step was the tetrahedral intermediate formation. The linear correlation between the calculated DFT and experimental rates for *N*-methylmaleamic acids **1–7** provided a credible basis for designing tranexamic acid prodrugs that have the potential to release the parent drug in a sustained release fashion. For example, based on the calculated B3LYP/6-31G(d,p) rates the predicted $t_{1/2}$ (a time needed for 50 % of the prodrug to be converted into drug) values for tranexamic acid prodrugs **ProD 1–ProD 4** at pH 2 were 556 h [50.5 h as calculated by B3LYP/311+G(d,p)] and 6.2 h as calculated by GGA: MPW1K), 253 h, 70 s and 1.7 h, respectively. Kinetic study on the interconversion of the newly synthesized tranexamic acid prodrug **ProD 1** revealed that the $t_{1/2}$ for its conversion to the parent drug was largely affected by the pH of the medium. The experimental $t_{1/2}$ values in 1 N HCl, buffer pH 2 and buffer pH 5 were 54 min, 23.9 and 270 h, respectively.

R. Karaman (✉) · H. Ghareeb · H. Hallak · S. Abu-Lafi
Bioorganic Chemistry Department, Faculty of Pharmacy,
Al-Quds University, P. O. Box 20002, Jerusalem, Israel
e-mail: dr_karaman@yahoo.com

R. Karaman · L. Scrano · S. A. Bufo
Department of Sciences, University of Basilicata,
Via dell'Ateneo Lucano 10, 85100 Potenza, Italy

K. K. Dajani
Faculty of Public Health Sciences, Al-Quds University,
Box 20002, Jerusalem, Israel

G. Mecca
Exo Research Organization, Potenza, Italy

Introduction

Tranexamic acid is a synthetic lysine amino acid derivative. It was originally developed to prevent and reduce excessive hemorrhage in hemophilia patients and reduce the need for replacement therapy during and following tooth extraction. It is often prescribed for excessive bleeding. The mechanism by which tranexamic acid exerts its antifibrinolytic activity is by competitively inhibits the activation of plasminogen to plasmin, a molecule responsible for the degradation of fibrin. Tranexamic acid has roughly 8 times the antifibrinolytic activity of an older analogue, ε-aminocaproic acid [1]. Over the past few years, the use of tranexamic acid has been expanding beyond the small number of hemophilia patients; it is an important agent in decreasing mortality rate due to bleeding in trauma patients; this can be seen from CRASH-2 study which concludes that all cause mortality, relative risk and relative death due to bleeding were reduced with tranexamic acid

group more than placebo group [2]. In addition, tranexamic acid was found to reduce blood loss during and after surgery in women who undergo lower segment cesarean section [3]. Finally, tranexamic acid was shown to be pharmacologically active in reducing the need for intra-operative blood transfusion during heart surgery, hip and knee replacement surgery and liver transplant surgery [4].

Tranexamic acid pharmacokinetic profile indicates that after an intravenous dose of 1 g the plasma concentration time curve shows a terminal elimination half-life of about 2 h [1]. Furthermore, tranexamic acid in CRASH-2 study was administered using a loading dose of 1 g by intravenous infusion over 10 min followed by 1 g infusion over 8 h. Although an 8 h IV infusion may be an easy option in a hospital setting, such option may not be available in under-developed countries [2].

Recently, a new oral formulation of tranexamic acid was shown to be safe and effective for treatment of heavy menstrual bleeding [5]. Oral administration of tranexamic acid results in a 45 % oral bioavailability. The total oral dose recommended in women with heavy menstrual bleeding was two 650 mg tablets 3 times daily for 5 days. Accumulation following multiple dosing was reported to be minimal [6].

Post-partum hemorrhage is a leading cause of maternal mortality, accounting for about 100,000 maternal deaths every year. Medications used to control postpartum hemorrhage (PPH) are in the category of uterotonic drugs. These drugs stimulate contraction of the uterine muscle, helping to control PPH. The two medications most commonly used for treatment include oxytocin or misoprostol. In addition, patients are commonly given an IV blood transfusion in cases of severe hemorrhage [7, 8]. In third world countries, availability of blood and fluid replacement may be an issue. One approach to decrease the risk of maternal hemorrhage may be to improve the availability of blood and fluid replacement. An alternative approach is to decrease the likelihood of maternal hemorrhage. Furthermore, all the treatment options mentioned above are intended for intravenous administration; this may not be a viable option in under-developed countries. Therefore, a cheaper oral alternative may be better suited for such circumstances.

Several preliminary studies were conducted to evaluate the effect of tranexamic acid in PPH. Recent analysis of the available data indicates that two studies provided the most reliable data. Both studies explored the efficacy and safety of tranexamic acid at caesarian section (CS). Tranexamic acid was administered via slow IV infusion (over 5 min) at a dose of 1 g, 10 min before incision. Both studies concluded that tranexamic acid statistically reduces the extent of bleeding from placental delivery to 2 h postpartum and its use was not associated with any side effects or

complications. Thus, tranexamic acid can be used safely and effectively to reduce bleeding resulting from CS [9–11].

After the withdrawing of aprotinin from worldwide market in November 2009, tranexamic acid is the only marketed antifibrinolytic agent available in the market [12].

Further, it was found that tranexamic acid is also effective in inhibiting the activity of urokinase in urine [13] and it is safe and effective for treating severe hematourea in patient with chronic renal impairment that poorly respond to conventional therapy [14].

Recent studies showed that tranexamic acid inhibits the ultraviolet radiation induced pigmentation activity, thus it can be used as bleaching agents [15]. Oral tranexamic acid dosage form was found to be effective and safe in treating melasma, a hypermelanosis disease that occurs in Asian women [16].

Since tranexamic acid is an amino acid derivative and undergoes ionization in physiologic environments its oral bioavailability is expected to be low due to inefficient absorption through membranes. Note the log P (partition coefficient) for tranexamic acid is −1.6 [17]. Hence, there is a necessity to design and synthesis a relatively more lipophylic tranexamic acid prodrugs that can provide the parent drug in a sustained release manner which might result in better clinical outcome, more convenient dosing regimens and potentially less side effects than the original medication.

In general, such tranexamic acid derivatives need to be pharmacologically inactive chemicals that could be used to alter the physicochemical properties of tranexamic acid, in a temporary manner. To enhance the oral pharmacokinetic properties of tranexamic acid and increase its usefulness, lipophylic linkers need to covalently bound to the parent drug and such linkers need to e able to be converted in vivo to the active drug molecule, enzymatically or nonenzymatically, to exert a therapeutic effect. Ideally, the prodrugs should be converted to the original drug as soon as the goal is achieved, followed by the subsequent rapid elimination of the released linker group. For example, tranexamic acid is given by continuous IV infusion resulting in peak plasma concentration following administration. If an IV slow release prodrug can be prepared, then tranexamic acid C_{max} related side effects may be avoided and longer duration of exposure may be achieved resulting in potentially better maintenance paradigm.

In addition, improvement of tranexamic acid pharmacokinetic properties and hence its effectiveness may increase the absorption of the drug via a variety of administration routes, especially the oral and SC injection routes of administration.

Modern computational methods can be used for the design of innovative prodrugs for medicines that contain

hydroxyl or amine groups. For example, mechanisms of some enzyme models that have been used to gain a better understanding of enzyme catalysis have been recently investigated and utilized for the design of novel prodrug linkers [18–36]. Using computational methods such as density functional theory (DFT), molecular mechanics and ab initio, various enzyme models were investigated for assigning the factors affecting the rate-determining step and playing dominant roles in governing the reaction rate. Among these enzyme models are: (a) proton transfer between two oxygens in Kirby's acetals [37–43] and proton transfer between ammonium nitrogen and oxygen in Kirby's enzyme model [37–43]; (b) intramolecular acid-catalyzed hydrolysis in some of Kirby's N-alkylmaleamic acid derivatives [37–43]; (c) proton transfer between carboxylic oxygen and alcoholic oxygen in rigid systems as investigated by Menger [44–47]; (d) the acid-catalyzed lactonization of hydroxy-acids as studied by Milstein and Cohen [48–50] and Menger [44–47]; and (e) the S_N2-based ring closing reactions as studied by Brown, Bruice, and Mandolini [51–54].

These studies have revealed to the followings: (1) rates acceleration in intramolecular processes is a result of both entropy and enthalpy effects. In intramolecular ring-closing reactions where enthalpic effects were predominant, steric effects were the determining factor for the acceleration, whereas proximity orientation was the determining factor in proton-transfer reactions. (2) The distance between the two reacting centers is the main factor in determining whether the reaction type is intermolecular or intramolecular. When the distance exceeded 3 Å, an intermolecular engagement was preferred because of the engagement with a water molecule (solvent). When the distance between the electrophile and nucleophile was <3 Å, an intramolecular reaction was dominant. (3) The efficiency of proton transfer between two oxygens and between nitrogen and oxygen in Kirby's enzyme models is attributed to a relatively strong hydrogen bonding in the products and the transition states leading to them [18–36].

It was concluded from the studies on intramolecularity that there is a need to further investigate the reaction mechanism for assigning the factors determining the reaction rate. This would allow for better design of an efficient chemical device that can be used as a prodrug linker and have the potential to chemically and not enzymatically liberate the active drug in a programmable or controlled manner. Among the various approaches to minimize the undesirable drug properties while retaining the desirable therapeutic activity, the chemical approach using drug derivatization offers perhaps the highest flexibility and has been demonstrated as an important means of improving drug efficacy. The prodrug approach can be useful in the optimization of the clinical application of a drug. Numerous prodrugs have been designed and developed to overcome pharmaceutical and pharmacokinetic barriers in clinical drug application, such as low oral drug absorption, lack of site specificity, chemical instability, toxicity, and poor patient acceptance (bad taste, odor, pain at injection site, etc.). However, till now no experimental study has been reported for prodrug systems consisting of a covalently linked drug to a host (prodrug) that is capable of releasing the parental drug via a controlled cleavage reaction.

It is worthy to note that our previous studies [18–36] on enzyme models emphasize the necessity to explore the reaction mechanism and to assign the driving force affecting the reaction rate in order to design an efficient chemical device (pro-drug). The designed prodrugs should have the potential to undergo cleavage reactions in physiological environments at rates that are completely dependent on the structural features of the host (inactive linker). By doing so, a variety of linkers could be used to obtain different prodrugs that release the parental drug at different rates depending mainly on the nature or the structural features of the linker.

Continuing our study on how to utilize enzyme models as potential carriers for drugs containing amine and hydroxyl groups [55–60], we sought to study the proton transfer reactions in the acid-catalyzed hydrolysis of N-alkylmaleamic acids 1–7 (Kirby's enzyme model, Fig. 1) reported by Kirby and Lancaster [61]. Based on the calculation results of this system, we propose four tranexamic acid prodrugs, tranexamic prodrugs **ProD 1**–**ProD 4** (Fig. 2).

As shown in Fig. 2, tranexamic acid prodrugs, **ProD 1**–**ProD 4** have a carboxylic group (hydrophilic moiety) and a lipophilic moiety (the rest of the prodrug), where the combination of both moieties secures a relatively moderate HLB.
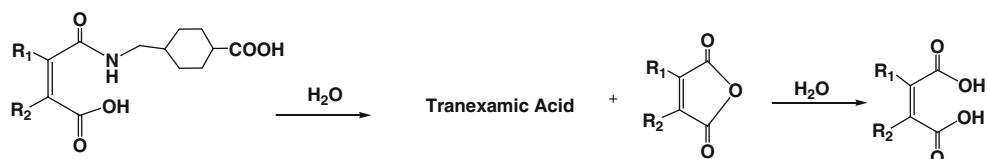
In most of the physiologic environments (pH 1–8.0) tranexamic acid will exist primary in the ionized forms (Eq. 1) while its prodrugs, **ProD 1**–**ProD 4**, will equilibrate between the ionic and the free acid forms (Eq. 2) especially in the physiological pH environment of 5.5–6.8 (intestine). Thus, it is expected that prodrugs **ProD 1**–**ProD 4** may have a better bioavailability and pharmacokinetic profile than that of the parent drug due to neutralizing the ionization of the amine group which results in the oral absorption improvement. In addition, these prodrugs may be used in different dosage forms (i.e. enteric coated tablets, topical use and etc.) because of their potential solubility in organic and aqueous media due to the ability of the carboxylic group to be converted to the corresponding carboxylate anion in a physiological pH of around 6.0.

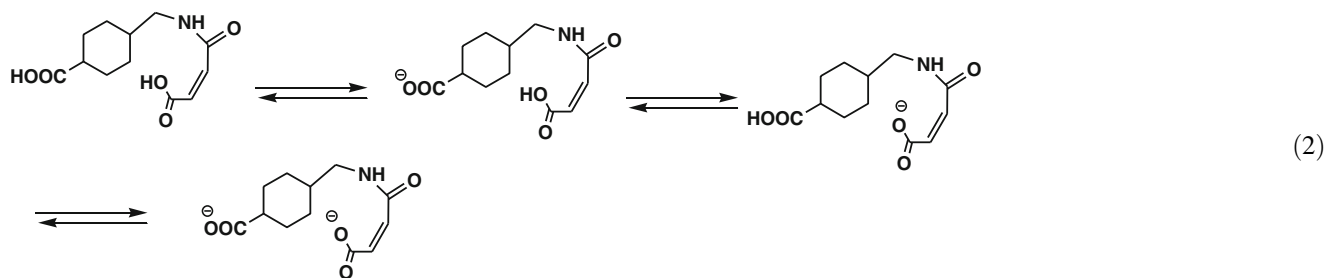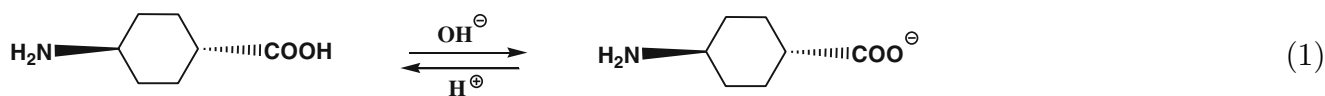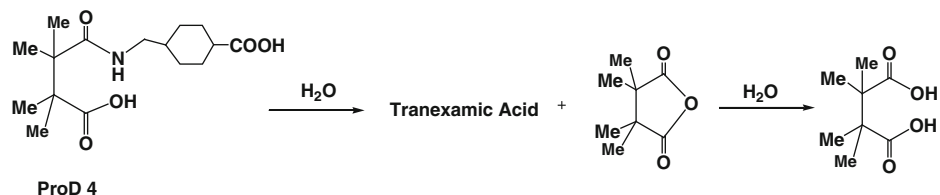**Fig. 1** Acid-catalyzed hydrolysis in Kirby's *N*-methylmaleamic acids **1–7**
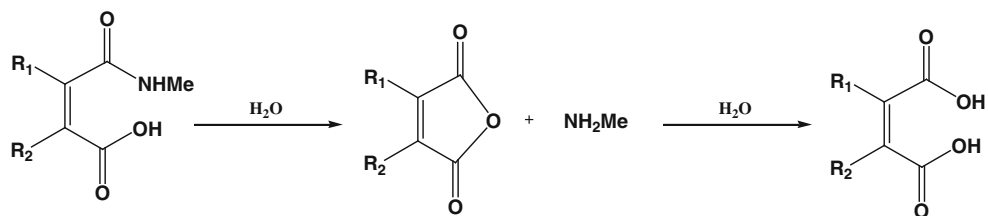
1; $R_1=R_2=H$
2; $R_1=R_2=Me$
3; $R_1=H$; $R_2=Me$
4; R_1,R_2 Cyclopent-l-ene-1,2-diyl
5; R_1, R_2 Cyclohex-l-ene-1,2-diyl
6; $R_1=H$; $R_2=Et$
7; $R_1=H$; $R_2=n$-Propyl

Fig. 2 Acid-catalyzed hydrolysis in tranexamic acid prodrugs, **ProD 1–ProD 4**

ProD1; $R_1=R_2=H$
ProD2; $R_1=R_2=Me$
ProD3; $R_1=H$; $R_2=Me$

ProD 4

(1)

(2)

It should be emphasized that at pH 5.5–6.5 (SC, skin, mouth cavity and intestine physiologic environments) the carboxylic group of the prodrugs will equilibrate with the corresponding carboxylate form (Eq. 2). Subsequently, the free acid form will undergo proton transfer reaction (rate limiting step) to yield the antifibrinolytic drug, tranexamic acid, and the inactive linker as a by-product (Fig. 2).

It is worth noting that our proposal is to exploit tranexamic acid prodrugs **ProD 1**–**ProD 4** for oral use via enteric coated tablets. At this physiologic environment these prodrugs will exist in the acidic and ionic forms where the equilibrium constant for the exchange between the two forms is dependent on the pK_a of the given prodrug (Eq. 2). The experimentally determined pK_a for tranexamic acid **ProD 1**–**ProD 4** linkers are in the range of 4–6. Therefore, it is expected that the pK_as of the corresponding prodrugs will have similar pK_a range as for the carboxylic linkers. Since the pH for the small intestine lies in the range of 5.5–6.8, the calculated unionized (acidic)/ionized ratio will be in the range of 10–50 %. Although the percentage of the acidic form is not significantly high, we expect these prodrugs to undergo an efficient proton transfer (rate limiting step) to yield the antifibrinolytic drug, tranexamic acid especially **ProD 4** that have a pK_a close to 6.5. In the blood circulation at pH 7.4, the calculated acidic form is around 1 % and it is expected that the efficiency for delivering the parent drug will be relatively low. Improving the efficiency could be achieved by using carboxylic linkers having pK_a close to that of the blood circulation (pH 7.4).

In this manuscript, we describe our theoretical and experimental study which includes: (1) DFT quantum molecular orbital investigations of ground and transition states structures, vibrational frequencies, and reaction trajectories for the intramolecular proton transfer in seven *N*-methylmaleamic acids, **1**–**7**, and four proposed tranexamic acid prodrugs **ProD 1**–**ProD 4** (Figs. 1, 2). It is expected that the study on proton transfers in these systems will provide a good basis for the prediction of the pharmacokinetic behavior of the prodrugs of the type **ProD 1**–**ProD 4** and (2) synthesis, characterization and kinetic study of the interconversion of tranexamic acid **ProD 1** in different media; 1 N HCl. Buffer pH 2, buffer pH 5 and buffer pH 7.4.

Calculations methods

The Becke three-parameter, hybrid functional combined with the Lee, Yang, and Parr correlation functional, denoted B3LYP, were employed in the calculations using DFT. The DFT calculations at B3LYP/6-31G(d,p) and B3LYP/311+G(d,p) levels, MP2 calculations and the density functional from Truhlar group (hybrid GGA: MPW1k) [62–64] were carried out using the quantum chemical package Gaussian-2009 [65]. Calculations were carried out based on the restricted Hartree–Fock method [65]. The starting geometries of all calculated molecules were obtained using the Argus Lab program [66] and were initially optimized without the presence of water, with one

water molecule and with two water molecules at the HF/6-31G level of theory, followed by optimization at the B3LYP/6-31G(d,p), B3LYP/6-311+G(d,p), MPW1k [mpwpw91/6-31+G(d,p)] or MP2/6-31G(d,p) levels. Total geometry optimizations included all internal rotations. Second derivatives were estimated for all 3N-6 geometrical parameters during optimization. The search for the global minimum structure in each of **1**–**7** and tranexamic acid **ProD 1**–**ProD 4** was accomplished by 360° rotation of the carboxylic group about the C6–C7 bond (i.e. variation of the dihedral angle O1/C7/C6/C5, Fig. 3), and 360° rotation of the carbonyl amide group about the C4–C5 bond (i.e. variation of the dihedral angle O3/C4/C5/C6) in increments of 10° and calculation of the conformational energies (see Fig. 3). For systems **1**–**7**, and tranexamic acid prodrugs **ProD 1**–**ProD 4** two types of conformations in particular were considered: one in which the amide carbonyl is *perpendicular* to the carboxyl carbonyl group and another in which it is *planar*. An energy minimum (a stable compound or a reactive intermediate) has no negative vibrational force constant. A transition state is a saddle point which has only one negative vibrational force constant [67]. Transition states were located first by the normal reaction coordinate method [68] where the enthalpy changes was monitored by stepwise changing the interatomic distance between two specific atoms. The geometry at the highest point on the energy profile was re-optimized by using the energy gradient method at the B3LYP/6-31G(d,p) level of theory [65]. The "reaction coordinate method" [68] was used to calculate the activation energy in all maleamic (4-amino-4-oxo-2-butenoic) acid amides (Figs. 1–2). In this method, one bond length is constrained for the appropriate degree of freedom while all other variables are freely optimized. The activation energy values for the approach processes in **1**–**7** and tranexamic acid prodrugs **ProD 1**–**ProD 4** (the approach of O1 towards C4, Fig. 3) were calculated from the difference in energies of the global minimum structures (GM) and the derived transition states (tetrahedral intermediate formation). In the same manner, the activation energies of the dissociation processes in **1**–**7** and tranexamic acid prodrugs **ProD 1**–**ProD 4** (the breakdown of C4–N9 bond, Fig. 3) were calculated from the difference in energies of the global minimum structures (GM) and the corresponding transition states (tetrahedral intermediate breakdown). Full optimization of the transition states was accomplished after removing any constrains imposed while executing the energy profile. The activation energies obtained from the DFT at B3LYP/6-31G(d,p) level of theory for all molecules were calculated, in the presence of one water molecule, with and without the inclusion of water (dielectric constant of water, 78.39). The calculations with the incorporation of a water molecule were performed using

Fig. 3 Chemical representation of the *perpendicular* and *planar* conformations for the global minimum structures (GM) of **1–7** and tranexamic acid prodrugs **ProD 1–ProD 4**

Perpendicular   **Planar**
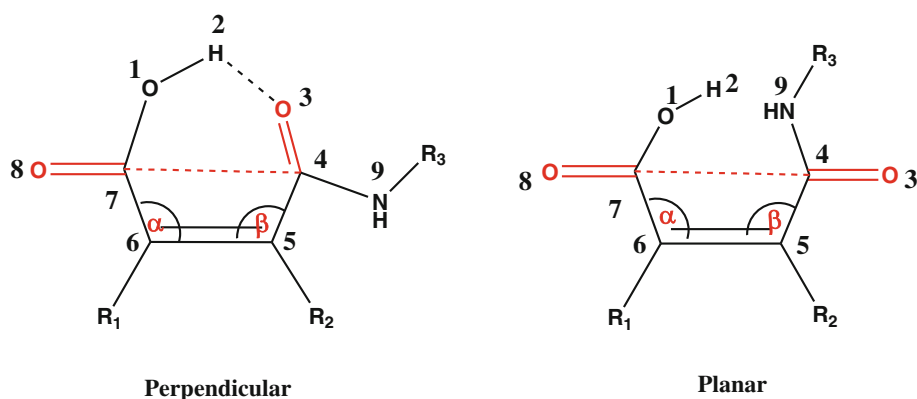
the integral equation formalism model of the Polarizable Continuum Model (PCM) [69–72]. In this model the cavity is created via a series of overlapping spheres. The radii type employed was the United Atom Topological Model on radii optimized for the PBE0/6-31G(d) level of theory.

Experimental

General

Inorganic salts were of analytical grade and were used without further purification. Organic buffer components were distilled or recrystallized. Distilled water was redistilled twice before use from all-glass apparatus. Maleic anhydride, anhydrous sodium dihydrogen phosphate, sodium lauryl sulfate, triethyl amine and tranexamic acid were commercially obtained from sigma Aldrich. HPLC grade solvents of methanol, acetonitrile and water were purchased from Sigma Aldrich. High purity chloroform, THF and diethyl ether (>99 %) were purchased from Biolab (Israel). The LC/ESI–MS/MS system used was Agilent 1200 series liquid chromatography coupled with a 6520 accurate mass quadruple-time of flight mass spectrometer (Q-TOF LC/MS). The analysis was performed in the positive electrospray ionization mode. The capillary voltage was 4.0 kV, the scanned mass range was 200–540 m/z (MS).

The high pressure liquid chromatography (HPLC) system consisted of an Alliance 2695 module equipped with 2996 Photodiode array detector from Waters (Germany). Data acquisition and control were carried out using Empower 2™ software (Waters, Germany). Analytes were separated on a 4.6 mm × 150 mm XBridge® C18 column (5 μm particle size) used in conjunction with a 4.6 × 20 mm, XBridge® C18 guard column. Microfilters of 0.45 μm porosity were normally used (Acrodisc® GHP, Waters). pH meter model HM-30G: TOA electronics™ was used in this study to measure the pH value for the

buffers. The Sep-Pack C18 6 cc (1 g) cartridges were purchased form Waters (Milford, MA, USA). ^{1}H-NMR experiments were performed with a Bruker AvanceII 400 spectrometer equipped with a 5 mm BBO probe. All infrared spectra (FTIR) were obtained from a KBr matrix (4,000–400 cm^{-1}) using a PerkinElmer Precisely, Spectrum 100, FT-IR spectrometer.

Preparation of tranexamic acid ProD 1 (Scheme 1)

In a 250 mL round-bottom flask, tranexamic acid (10 mmol) was dissolved in THF (100 mL), a solution of 0.5 g NaOH in dry THF was added (50 mL), the resulting solution was stirred for 30 min, then maleic anhydride (10 mmol) was slowly added to the reaction mixture and stirred at room temperature for 10 h, then the reaction mixture was refluxed for 2 h and cooled to room temperature. The white precipitate formed was collected and dried (yield 87 %). M.P. 201 °C (not corrected). ^{1}H-NMR δ (ppm) CD$_3$OD– 1.03–1.06 (q, 2H, J = 3.2 Hz, CH–C$\underline{H_2}$–CH$_2$), 1.36–1.40 (q, 2H, J = 3.6 Hz, CH–C$\underline{H_2}$–CH$_2$), 1.54–1.56 (m, 1H, CH$_2$–C$\underline{H}$–CH$_2$–CH$_2$), 1.84–1.89 (m, 2H, CH$_2$–C$\underline{H_2}$–CH), 1.99–2.02 (m, 2H, CH$_2$–C$\underline{H_2}$–CH), 2.03–2.22 (m, 1H, CH$_2$–C$\underline{H}$–CH$_2$–CH$_2$), 3.16–3.17 (d, 2H, J = 6.8 Hz, C$\underline{H_2}$–N), 6.23–6.25 (d, 1H, J = 12.8 Hz, HC = C$\underline{H}$), 6.27–6.44 (d, 1H, J = 12.8 Hz, $\underline{H}$C = CH). IR (KBr/v_{max} cm^{-1}) 1,712 (C = O), 1,643 (C = O), 1,587 (C = C), 1,420, 1,280, 1,200, 1,132, 1,058. m/z 256.1179 (M + 1)$^+$ (for further details see Supplementary data).

Kinetic methods

Buffer preparation 6.8 g potassium dihydrogen phosphate were dissolve in 900 mL water for HPLC, the pH of buffer 2 was adjusted by diluted *o*-phosphoric acid and water was added to a final volume of 1,000 mL (0.05 M). The same procedure was done for the preparation of buffers pH 5 and 7.4, however, the required pH was adjusted using 1 N NaOH.
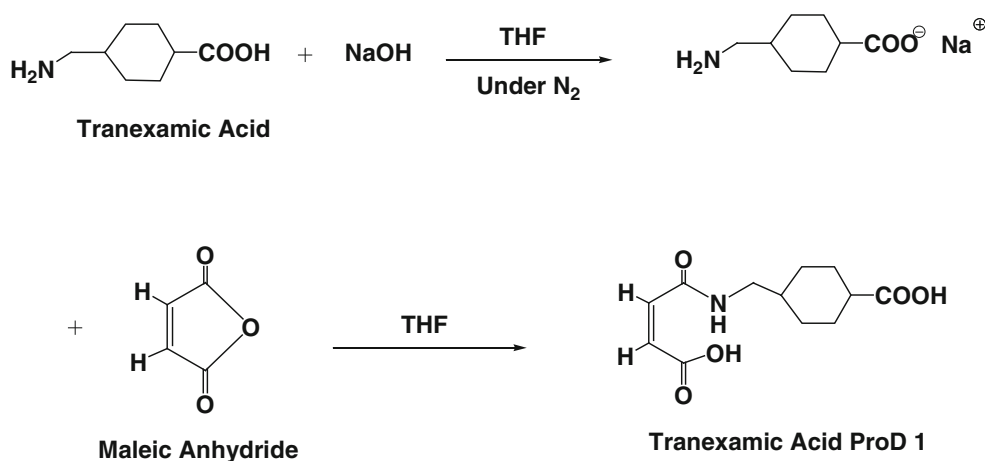
Scheme 1 Synthesis of tranexamic acid **ProD 1** from its parent drug, tranexamic acid

Interconversion of 500 ppm tranexamic acid **ProD 1** solution, in 1 N HCl, buffer pH 2, buffer pH 5 or buffer pH 7.4, to its parent drug, tranexamic acid, was followed by HPLC monitoring at a wavelength of 220 nm. Conversion reactions were run mostly at 37.0 °C.

Calibration curve for tranexamic acid and tranexamic acid prodrug **ProD 1** To construct a calibration curve for tranexamic acid **ProD 1** and the parent drug, tranexamic acid, several concentrations (0.1, 1.0, 2.0, 5.0, 10.0, 20.0, 50, 100 and 200.0 ppm) were prepared. 20 μL of each solution was injected into the HPLC and the peak for the pharmaceutical was recorded using the following HPLC conditions: 4.6 mm × 250 mm, 5 μm, XBridge® C18 column using mobile phase containing 11 g anhydrous sodium dihydrogen phosphate, 1.4 g Sodium Lauryl Sulfate, 5 mL triethyl amine dissolved in 600 mL water and 400 mL methanol (pH 2.5 using diluted phosphoric acid), a flow rate of 0.9 mL/min and UV detection at a wavelength of 220 nm.

Peak area versus concentration of the pharmaceutical (ppm) was then plotted, and R^2 value of the plot was recorded.

Preparation of standard and sample solution 500 ppm of standard tranexamic acid was prepared by dissolving 50 mg of drug in 100 mL of 1 N HCl, buffer pH 2, buffer pH 5 or buffer pH 7.4, then each sample was injected into HPLC to detect the retention time of tranexamic acid.

500 ppm of standard maleic anhydride was prepared by dissolving 50 mg of drug in 100 mL of 1 N HCl, buffer pH 2, buffer pH 5 or buffer pH 7.4, then each sample was injected into HPLC to detect the retention time of maleic anhydride.

500 ppm of tranexamic acid **ProD 1** was prepared by dissolving 50 mg of the prodrug in 100 mL of 1 N HCl, buffer pH 2, buffer pH 5 or buffer pH 7.4 then each sample was injected into HPLC to detect the retention time.

The progression of reaction was followed by monitoring the disappearance of the prodrug peak and the appearance of tranexamic acid and maleic anhydride versus time.

Results and discussion

Kirby et al. studied the efficiency of intramolecular catalysis of amide hydrolysis by the carboxy-group of a number of substituted *N*-methylmaleamic acids, **1–7** (Fig. 1) and found that the reaction is remarkably sensitive to the pattern of substitution on the carbon–carbon double bond. In addition, their study revealed that the rates of hydrolysis of the studied dialkyl-*N*-methylmaleamic acids range over more than ten powers of ten, and the "effective concentration" of the carboxy-group of the most reactive amide, dimethyl-*N*-*n*-propylmaleamic acid, is greater than 10^{10} M. This acid amide was found to be converted into the more stable dimethylmaleic anhydride with a half-life of less than 1 s at 39 °C below pH 3 [61].

Furthermore, Kirby and Lancaster's [61] study demonstrated that the amide bond cleavage is due to intramolecular nucleophilic catalysis by the adjacent carboxylic acid group and the dissociation of the tetrahedral intermediate is the rate-limiting step. Later on Kluger and Chin [73] researched the intramolecular hydrolysis mechanism of a series of *N*-alkylmaleamic acids derived from aliphatic amines having a wide range of basicity. Their study revealed that the identity of the rate-limiting step is a function of both the basicity of the leaving group and the acidity of the solution.

To utilize *N*-alkylmaleamic acids, **1–7**, as prodrug linkers for atenolol, acyclovir, cefuroxime and other drugs having poor bioavailability or/and undesirable (bitter) taste, we have unraveled the mechanism for their acid-catalyzed hydrolysis using DFT and molecular mechanics methods.

Our DFT calculation results were found to be in accordance with the reports by Kirby and Lancaster [61] and Kluger and Chin [73]. Our findings demonstrated that the *N*-alkylmaleamic acids hydrolysis occurs by one mechanism where the rate-limiting step was found to be largely dependent on the nature of the amine leaving group and the medium solvent. Two different rate-limiting steps were proposed: one involves the formation of a tetrahedral intermediate [74], and the second involves a tetrahedral intermediate dissociation (Fig. 4) [61, 73]. The gas phase DFT calculations showed that the rate-limiting step for the hydrolysis of all maleamic acid amides studied regardless of the nature of the amine leaving group is a tetrahedral formation. On the other hand, when the DFT calculations were done in a dielectric constant of 78.39 (water) the rate-limiting step for the hydrolysis of acid amides having primary amine as a leaving group was the dissociation of the tetrahedral intermediate, whereas that having acyclovir or cefuroxime moieties the rate-limiting step was the tetrahedral intermediate formation.

In similar manner to that done for systems **1–7**, the DFT calculations for the acid-catalyzed hydrolysis of tranexamic acid prodrugs **ProD 1–ProD 4** were directed toward elucidation of the transition and ground state structures (reactants, intermediates and products). Calculations for all reaction entities were done, in the presence of one molecule of water, in a dielectric constant of 78.39 (water) and the gas phase. It is expected that the stability of the ground and transition states will be different in solvent having low dielectric constant, such as the gas phase and solvent with high dielectric constant, such as water.

General consideration

The ground state energy of the *N*-alkylmaleamic acid moiety is vastly affected by the orientation of both the carboxylic acid and amide groups especially when there is a possibility for engagement in intramolecular hydrogen bonding. Therefore, we were concerned with the identification of the most stable conformer (global minimum) for each of Kirby's *N*-alkylmaleamic acids **1–7** and tranexamic acid prodrugs **ProD 1–ProD 4**. The global minimum search was achieved by 360° rotation of the carboxylic group about the C6–C7 bond (i.e. variation of the dihedral angle O1C7C6C5, Fig. 3), and 360° rotation of the carbonyl amide group about the C4–C5 bond (i.e. variation of the dihedral angle O3C4C5C6) in increments of 10° and calculation of the conformational energies (see Fig. 3).

In the DFT calculations for **1–7** and tranexamic acid **ProD 1–ProD 4**, two types of conformers in particular

R-NH- = **Methylamine, Tranexamic acid, Atenolol, Aciclovir or Cefuroxime**
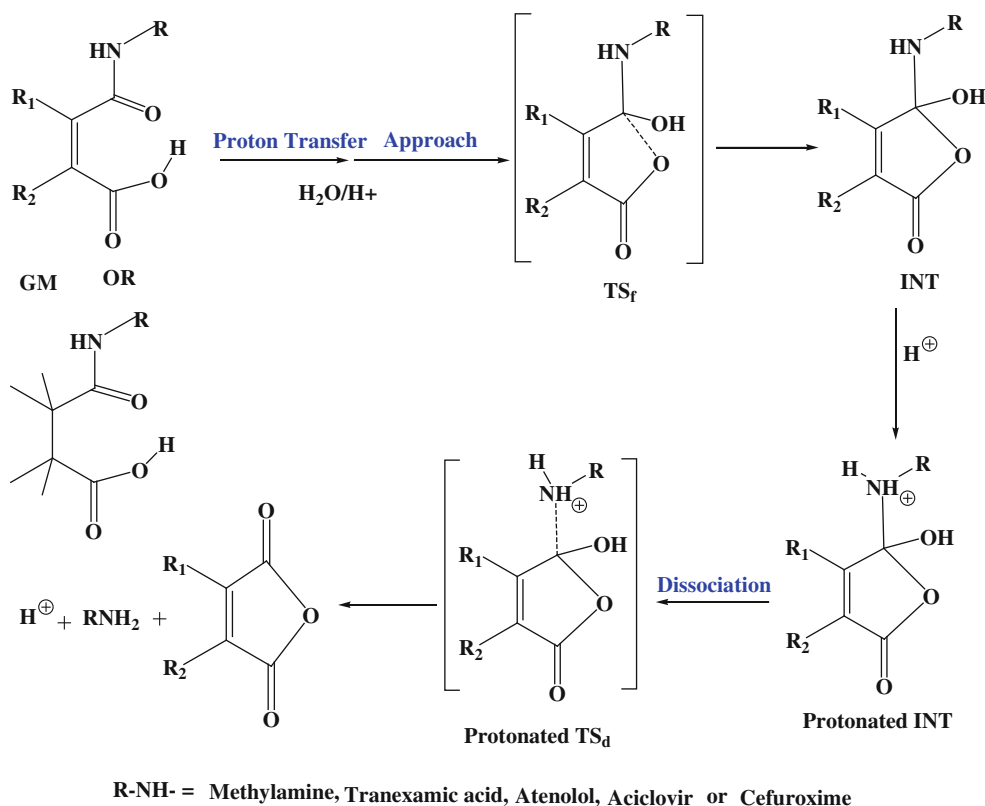
Fig. 4 Mechanistic pathway for the acid-catalyzed hydrolysis of **1–7** and tranexamic acid **ProD 1–ProD 4**. GM, INT, TS$_f$ and TS$_d$ are global minimum structure, tetrahedral intermediate 1, transition state for the formation step and transition state for the dissociation step, respectively

Fig. 5 a DFT optimized structures for the global minimum (GM) in tranexamic acid **ProD 1**–**ProD 4**. b DFT optimized structures for the tetrahedral intermediate (INT) in tranexamic acid **ProD 1**–**ProD 4**. c DFT optimized structures for the tetrahedral intermediate dissociation step (TS$_d$) in tranexamic acid **ProD 1**–**ProD 4**. d DFT optimized structures for the tetrahedral intermediate formation step (TS$_f$) in tranexamic acid **ProD 1**–**ProD 4**

Fig. 5 continued

ProD 1TS$_d$

ProD 2TS$_d$

ProD 3TS$_d$

ProD 4TS$_d$
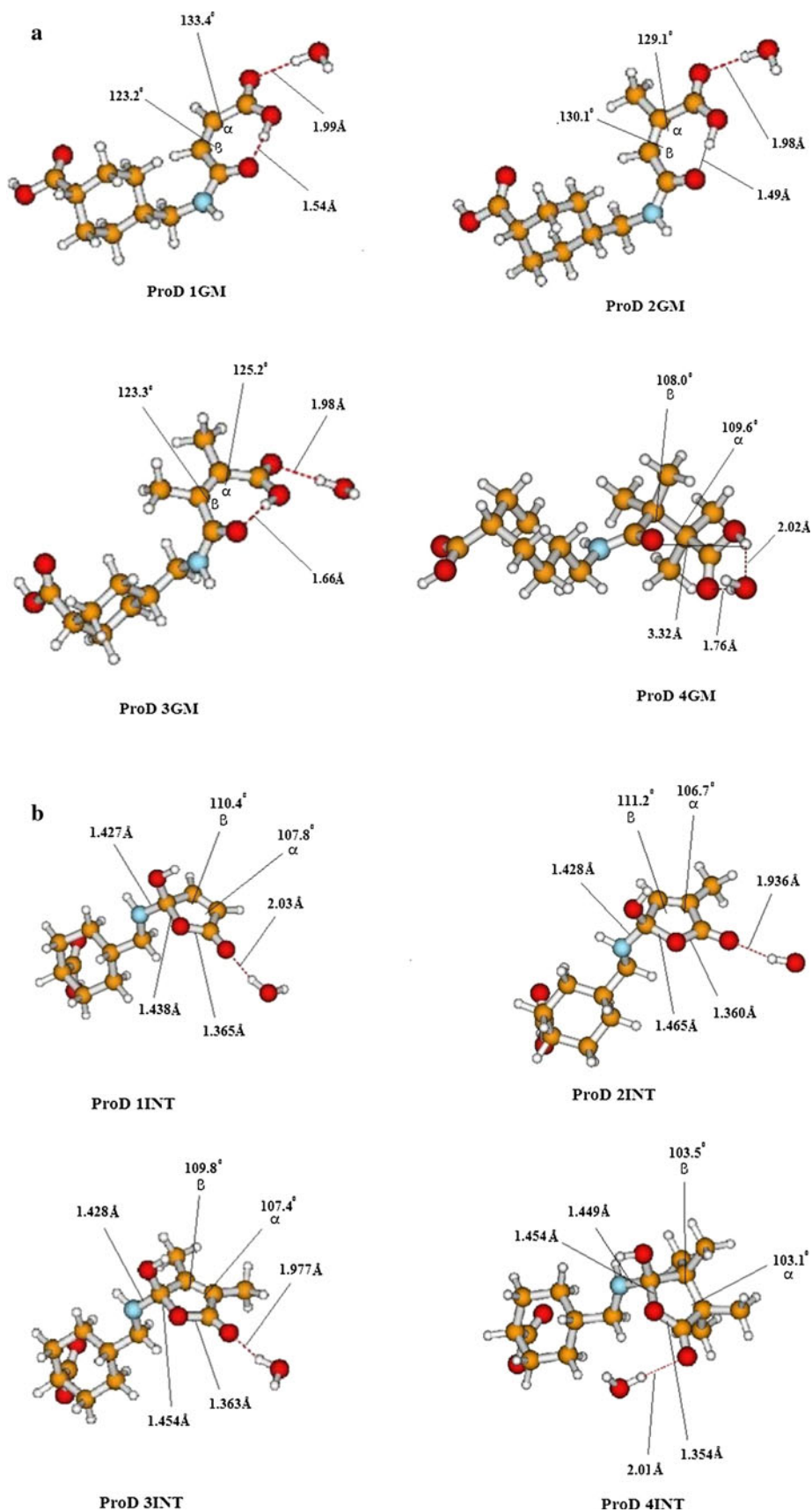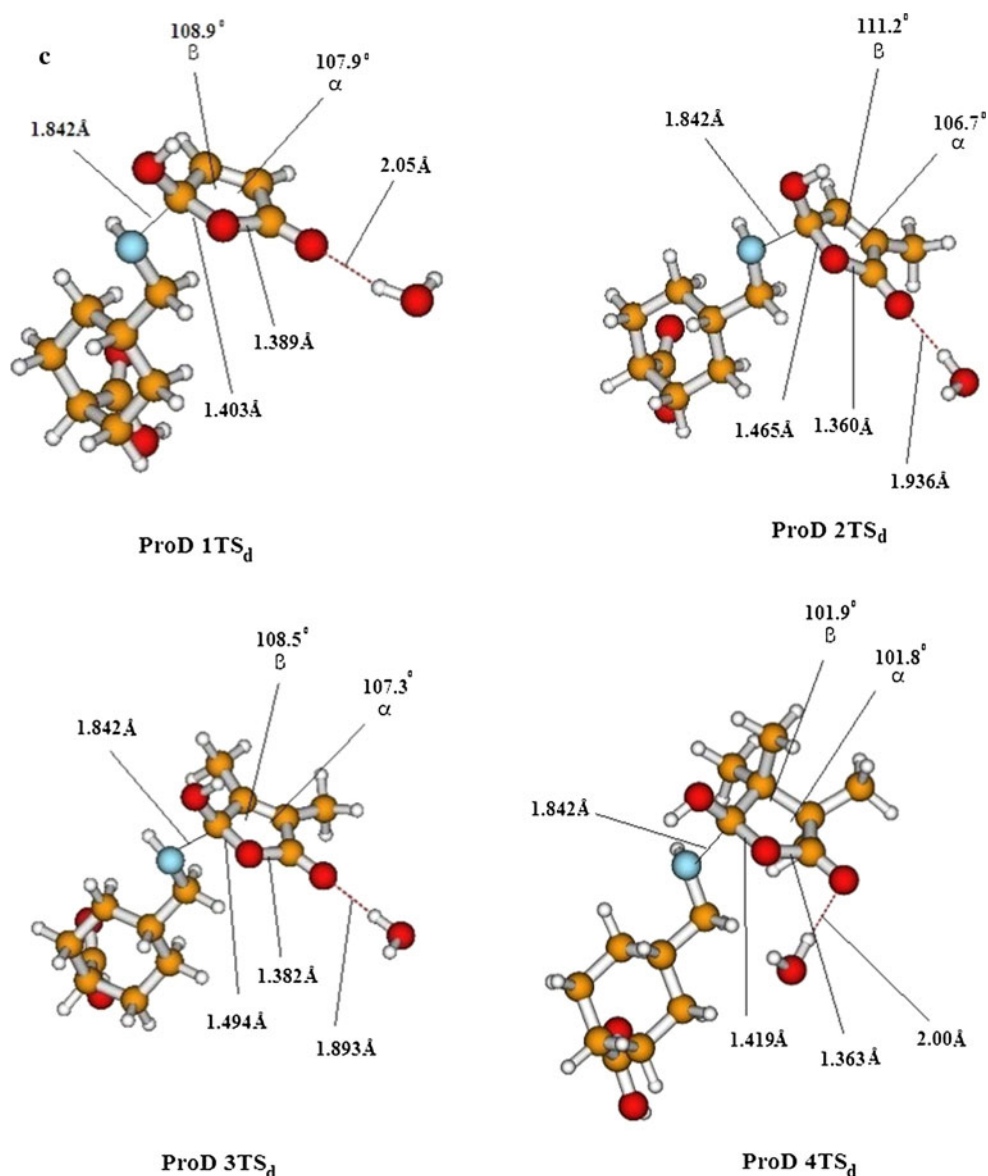
were considered: one in which the amide carbonyl is *perpendicular* to the carboxyl group and another in which it is *planar*. It was found that the global minimum structures for **1–7** and tranexamic acid **ProD 1–ProD 4** all exist in the *perpendicular* conformation (see Figs. 3, 5a).

Since the acid-catalyzed hydrolysis of *N*-alkylmaleamic acids involves two steps: tetrahedral intermediate formation and dissociation, it was our concern to examine if water molecules have any effect on the barriers involved in the reaction. Interaction of a water molecule with the carboxylic group might have an effect on its nucleophilicity. On the other hand, water molecule when interacts with the amide carbonyl group the ability of the *N*-alkyl amine as a leaving group might be altered. Therefore, the starting geometries for the reactants were calculated with one and two water molecules and without the presence of

water. The calculations were done by placing water molecule which is hydrogen bonded with the O8 (Fig. 3) of the carboxylic group such that the bond angle O8···H···O is in the range of 170–180. The calculations with two water molecules were executed by placing one water molecule that is hydrogen bonded with O8 of the carboxylic group and the other with O3 (Fig. 3) of the carbonyl amide group. The calculation results reveal that the presence of water has no significant effect on either the enthalpy or activation energies. For example, the gas phase calculated DFT enthalpic energy for system **2** without water, with one molecule of water and with two molecules of water were 12.96, 13.93 and 13.07 kcal/mol, respectively, whereas the calculated values in dielectric constant of 78.39 (water) were 16.93, 17.56 and 17.5 kcal/mol, respectively.

Fig. 5 continued

ProD 1TS$_f$

ProD 2TS$_f$

ProD 3TS$_f$

ProD 4TS$_f$
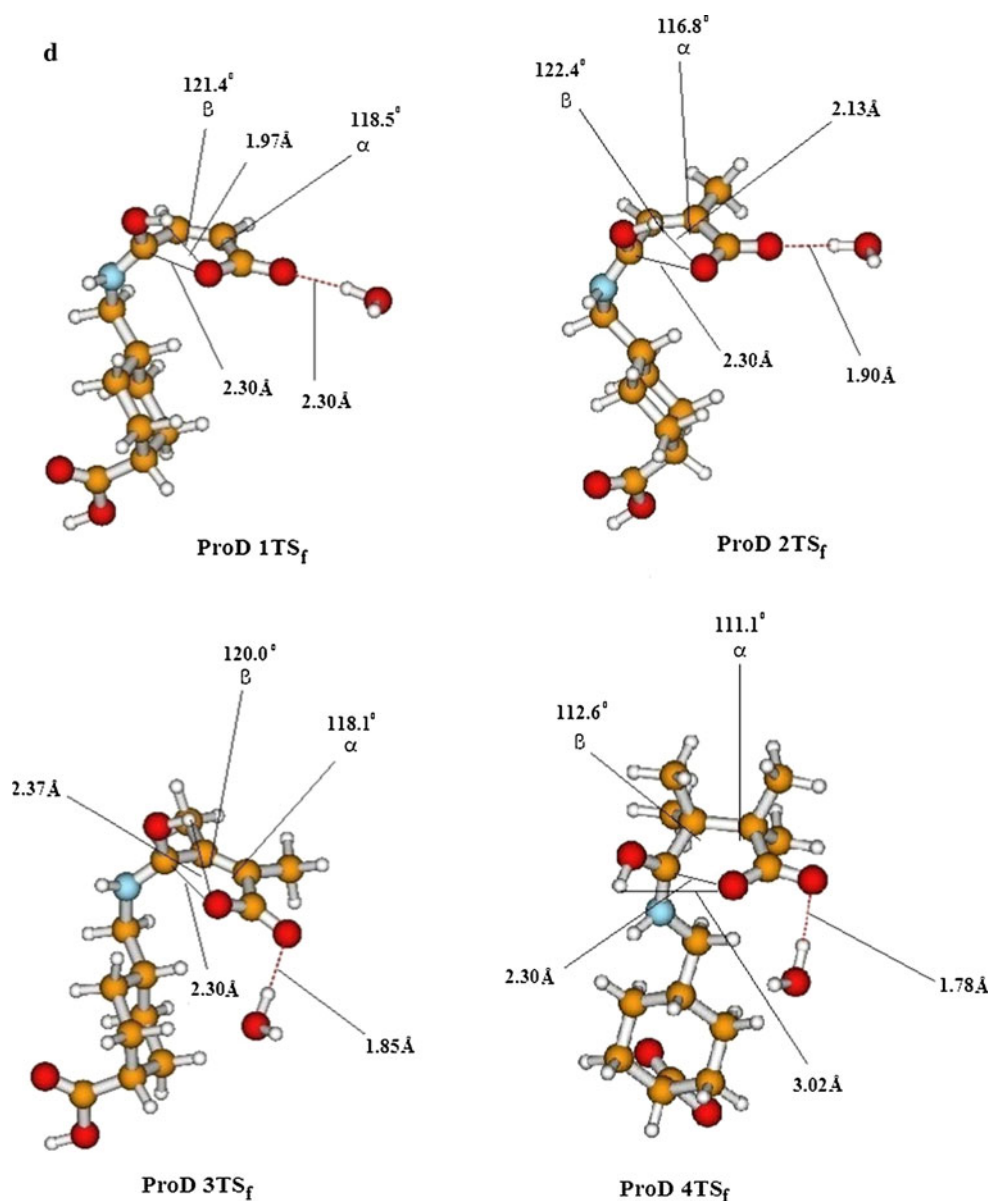
It should be emphasized that the orientation of the water molecules was positioned in a similar manner in all systems studied (**1–7** and **ProD 1–ProD 4**).

Optimized structures for the entities involved in the acid-catalyzed hydrolysis of tranexamic acid prodrugs ProD 1–ProD 4

Global minimum structures (GM) The global minimum structures for **ProD 1GM–ProD 4GM** are illustrated in Fig. 5a. Careful inspection of the calculated structures in Fig. 5a reveals that all the global minima of the reactants, except **ProD 4GM**, exist in conformation by which their carboxyl group is engaging intramolecularly in a hydrogen bonding net to form a seven-membered ring. Further, the

calculated DFT angles α and β values in the global minimum structures (**ProD 1GM–ProD 3GM**) were in the range of 125.2°–133.4° and 123.2°–130.1°, respectively. On the other hand the angle α and β values in tranexamic acid **ProD 4GM** were 109.6° and 108.0°, respectively.

Tetrahedral intermediate geometries (INT) The optimized structures for the tetrahedral intermediates, **ProD 1INT–4INT**, are shown in Fig. 5b. Inspection of the optimized structures demonstrates that angles α and β values in the intermediates are much smaller than the values of the corresponding angles in the reactants. The α range values was 103.1°–107.8° whereas that for the β was 103.5°–110.4°. Furthermore, the angles around the tetrahedral carbon were found to be similar to that of regular tetrahedral intermediates.

The ranges for O1–C7 and O1–C4 bond distances were 1.354–1.365 and 1.438–1.465 Å, respectively.

Transition state structures for the acid-catalyzed hydrolysis of tranexamic acid prodrugs ProD 1–ProD 4

The calculated DFT optimized structures for the transition states of the tetrahedral intermediate dissociation (rate-limiting step) in **ProD 1–ProD 4** (**ProD 1TS_d–ProD 4TS_d**) and tetrahedral formation (rate-limiting step) in **ProD 1–ProD 4** (**ProD 1TS_f–ProD 4TS_f**) are shown in Fig. 5c, d, respectively. Inspection of the DFT optimized transition state structures for **ProD 1TS_d–ProD 3TS_d** revealed that the geometries of the transition states resemble that of the corresponding tetrahedral intermediates. The angle α and β values are quite identical in both the tetrahedral intermediates and their corresponding transition states. The range of the α values were found in the range 106.7°–107.9° and that of β was in the range 108.5°–111.2°.

On the other hand, the rate-limiting step in the acid-catalyzed hydrolysis of tranexamic acid **ProD 4** was the tetrahedral intermediate formation and not its collapse. The transition state optimized geometries for the formation step in tranexamic acid **ProD 1–ProD 4** (**ProD 1TS_f–ProD 4TS_f**) are depicted in Fig. 5d. As shown in Fig. 5d, the calculated C–O distance (the distance between the nucleophile O– and the electrophile C) in **ProD 1TS_f–ProD 4TS_f** was 2.30 Å and the angle α and β were quite similar to that of the corresponding global minimum structures and were 111.1°–118.5° and 112.6°–122.4°, respectively.

It should be emphasized that the calculations for the entities involved in the acid-catalyzed hydrolysis for the systems studied in the presence of a water molecule and without water were comparable. When the calculated DFT activation energy values (Tables S1 and S2) in the presence and absence of a water molecule were examined for correlation strong correlation with a correlation coefficient r = 0.98 was obtained ($\Delta G^{\ddagger}$ (GP) = 0.8625 $\Delta G^{\ddagger}$ (H₂O) + 6.97).

Mechanistic investigation The DFT at B3LYP/6-31G(d,p) level of kinetic and thermodynamic properties for tranexamic acid prodrugs **ProD 1–ProD 4** (Fig. 2) were calculated using the quantum chemical package Gaussian-2009 [62]. The enthalpy and entropy energy values for all structures involved in the acid-catalyzed hydrolysis, global minimum (GM), transition states (TS), intermediates (INT) and products (P), were calculated, with the presence of a water molecule, in the gas phase and water (dielectric constant 78.39). Table 1 lists the enthalpy and entropy energy values for **ProD 1GM–ProD 4GM**, **ProD 1TS_f–ProD 4TS_f**, **ProD 1INT–ProD 4INT**, protonated **ProD 1INT–ProD 4INT**, **ProD 1TS_d–ProD 4TS_d** and protonated **ProD 1TS_d–ProD 4TS_d** and Fig. 5a–d illustrate their DFT optimized structures, respectively.

Using the calculated B3LYP/6-31G(d,p) enthalpy and entropy values for the GM and transition states involved in the acid-catalyzed hydrolysis of tranexamic acid prodrugs **ProD 1–ProD 4** the barriers ($\Delta G^{\ddagger}$) for all steps described in Fig. 4 were calculated in the gas phase as well as in water (dielectric constant of 78.39). The calculated DFT enthalpy and activation energy values for the barriers are listed in Table 2. Careful examination of the $\Delta G^{\ddagger}$ ($\Delta G^{\ddagger}_f$, activation energy for the tetrahedral intermediate formation and $\Delta G^{\ddagger}_d$, activation energy of the tetrahedral intermediate dissociation) values in Table 2 demonstrates that while the rate-limiting step for all prodrugs as calculated in the gas phase is the tetrahedral intermediate formation the picture is somewhat different when the calculations were done in water. The DFT calculations in water indicate that the rate-limiting step in the acid-catalyzed hydrolysis of tranexamic acid **ProD 4** was the tetrahedral intermediate formation while that for **ProD 1–ProD 3** was the tetrahedral intermediate collapse.

For an evaluation of the factors playing dominate role in determining the acid-catalyzed hydrolysis rate in tranexamic acid prodrugs **ProD 1–ProD 4** we have made a comparison of the calculated DFT properties for tranexamic acid prodrugs **ProD 1–ProD 4** with previously calculated properties for the acid-catalyzed hydrolysis of 1–7 (Fig. 1), atenolol Prodrugs **ProD 1–ProD 2** (Fig. 6) acyclovir prodrugs **ProD 1–ProD 4** (Fig. 6) and cefuroxime **ProD 1–ProD 4** (Fig. 6).

Table 2 lists the activation energy barrier values for the intermediate formation ($\Delta G^{\ddagger}_f$) and dissociation ($\Delta G^{\ddagger}_b$) for 1–7, atenolol Prodrugs **ProD 1–ProD 2**, acyclovir prodrugs **ProD 1–ProD 4** and cefuroxime **ProD 1–ProD 4**. Inspection of the energy values listed in Table 2 revealed that the rate-limiting step (higher barrier) in the gas phase for all systems studied is the tetrahedral intermediate formation (the energy barrier for the tetrahedral intermediate formation is about 0.5–20 kcal/mol higher than that for its breakdown). On the other hand, the picture is quite different when the calculations were done in dielectric constant of 78.39 (water medium). While for systems 1–7 and atenolol prodrugs **ProD 1–ProD 2** the rate-limiting step was the breakdown of the tetrahedral intermediate (energy difference between the breakdown and formation barriers is 3–9 kcal/mol) in the reactions of cefuroxime prodrugs **ProD 1–ProD 4** and acyclovir prodrugs **ProD 1–ProD 4** the rate-limiting step was found to be the formation of the tetrahedral intermediate (energy difference between the formation and break-down barriers is 14–30 kcal/mol).

Since the stability of the ground and transition states is largely dependent on the reaction solvent and based on

Table 1 DFT [B3LYP/6-31G(d,p)] calculated properties for the acid catalyzed hydrolysis of **tranexamic acid ProD 1–ProD 4**

Compound	Enthalpy, H (gas phase) (Ha)	Entropy, S (gas phase) (cal/mol-K)	Frequency(cm^{-1})
ProD 1GM[a]	−974.8819081	163.12	–
ProD 1TS$_f$[a]	−974.8326548	148.66	145.69i
ProD 1TETINT[a]	−974.8471076	150.98	–
ProD 1TETINT (protonated)	−898.7944564	137.23	
ProD 1TS$_d$[a]	−974.8065994	149.45	152.8i
ProD 1TS$_d$ (protonated)	−898.7843298	135.69	84.33
ProD 2GM[a]	−1,014.2048171	171.51	–
ProD 2TS$_f$[a]	−1,014.1594626	156.97	115.95i
ProD 2TETINT[a]	−1,014.1723376	157.60	–
ProD 2TETINT (protonated)	−938.2658956	146.56	
ProD 2TS$_d$[a]	−1,014.1327548	157.67	119.96i
ProD 2TS$_d$ (protonated)	−938.1152433	145.14	78.44
ProD 3GM[a]	−1,053.5140615	179.62	–
ProD 3TS$_f$[a]	−1,053.4868204	171.73	102.39i
ProD 3TETINT[a]	−1,053.4978521	163.08	–
ProD 3TETINT (protonated)	−977.4522428	154.44	
ProD 3TS$_d$[a]	−1,053.4581183	164.32	172.63i
ProD 3TS$_d$ (protonated)	−977.4423073	154.45	167.48
ProD 4GM[a]	−1,133.3773287	177.52	–
ProD 4TS$_f$[a]	−1,133.3096986	171.68	145.69i
ProD 4TETINT[a]	−1,133.3474671	175.66	–
ProD 4TETINT (protonated)	−1,057.2912653	154.43	
ProD 4TS$_d$	−1,133.3678845	173.21	41.02i
ProD 4TS$_d$ (protonated)	−1,057.2889832	161.75	79.44i

GM, TETINT and TS are global minimum, tetrahedral intermediate and transition state structures, respectively. f and d refer to tetrahedral intermediate formation and dissociation, respectively

[a] Calculated in the presence of a water molecule

Kirby's findings and our previous DFT calculations on this type of systems [24, 61], it is expected that the tetrahedral intermediate formation and dissociation barriers will be quite different when calculated in the gas phase or water. In fact, examination of the barriers values for the tetrahedral intermediate formation process ($\Delta G_f^{\ddagger}$) and tetrahedral

to shift the equilibrium to the reactants by destabilizing TS$_f$ and thus making the tetrahedral intermediate formation as the rate-limiting step whereas solvents with high dielectric constants such as water (78.39) interact via dipole–dipole interactions with the ionic transition state to shift the equilibrium to the right side (see Eq. 3).


$$(3)$$
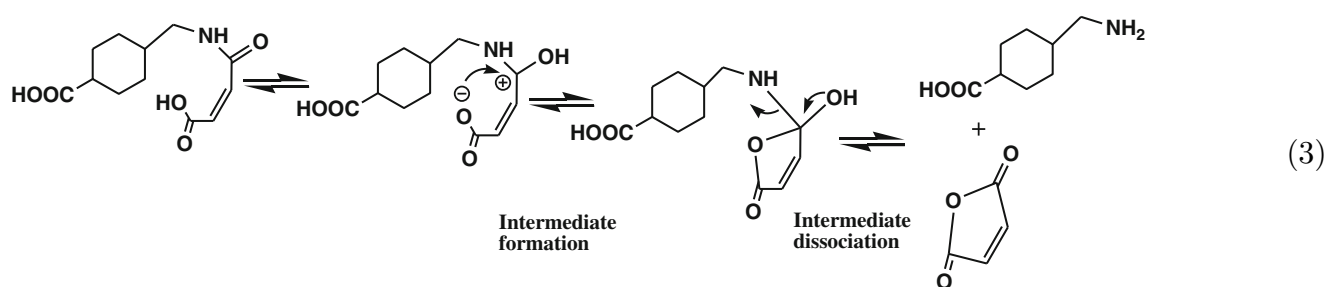
intermediate breakdown process ($\Delta G_d^{\ddagger}$) tabulated in Table 2 clearly indicates that solvents with low dielectric constant such as the gas phase (dielectric constant =1) tend

The dipole–dipole (hydrogen bonding) interactions stabilize the transition state for the tetrahedral intermediate formation (TS$_f$) which results in lowering the approach of

Table 2 DFT [B3LYP/6-31G(d,p)] calculated properties for the acid-catalyzed hydrolysis of **1–7**, tranexamic acid **ProD 1–ProD 4**, atenolol **ProD 1–ProD 2**, acyclovir **ProD 1–ProD 2**, acyclovir **ProD 1–ProD 4** and cefuroxime **ProD 1–ProD 4**

System	Es_{INT}	Es_{GM}	$\Delta H_f^{\ddagger}$ (GP)	$\Delta G_f^{\ddagger}$ (GP)	$\Delta H_f^{\ddagger}$ (H$_2$O)	$\Delta G_f^{\ddagger}$ (H$_2$O)	$\Delta H_d^{\ddagger}$ (GP)	$\Delta G_d^{\ddagger}$ (GP)	$\Delta H_d^{\ddagger}$ (H$_2$O)	$\Delta G_d^{\ddagger}$ (H$_2$O)	Log k_{rel} (Exp)	Log EM_{exp}	Log EM_{calc}
1	20.55	10.16	32.46	33.53	25.01	26.10	27.31	28.08	32.29	33.06	0	7.724	8.52
2	16.16	10.82	25.67	27.08	16.49	17.90	13.93	16.42	17.56	20.05	4.371	15.860	18.08
3	17.32	9.40	30.68	32.57	22.91	24.80	24.41	24.90	27.93	28.42	1.494	7.742	11.93
4	27.89	12.30	41.88	45.37	28.67	32.16	34.42	36.77	35.76	38.11	−4.377	1.255	4.81
5	19.25	9.18	24.55	26.87	15.57	17.89	13.25	17.41	18.96	23.12	2.732	15.190	15.82
6	17.59	5.12	30.11	32.12	21.86	23.87	23.83	23.92	27.19	27.28	1.516	6.962	12.76
7	18.55	6.20	30.76	32.30	22.86	24.40	24.86	25.03	27.38	27.55	1.648	8.568	12.57
TAProD 1	23.41	14.84	30.91	35.22	19.77	24.08	28.19	31.81	28.07	31.69	–	–	9.53
TAProD 2	21.58	15.02	28.46	32.79	16.63	20.99	26.59	30.71	27.12	31.24	–	–	9.86
TAProD 3	19.98	14.19	17.09	19.44	7.38	9.73	16.40	21.33	17.63	22.56	–	–	16.24
TAProD 4	25.60	19.06	42.44	44.18	23.41	25.15	18.76	19.31	18.20	18.75	–	–	14.33
AProD 1	41.97	20.97	29.96	35.95	29.77	35.76	20.08	27.86	31.37	39.12	–	–	–
AProD 2	38.42	17.31	31.94	30.75	19.04	17.85	15.43	15.25	26.98	26.80	–	–	–
ACProD 1	29.45	7.13	31.77	32.83	25.40	26.46	4.08	4.65	1.57	2.07	–	–	–
ACProD 2	42.27	32.70	32.10	34.12	29.48	31.50	0	0.66	0	0.66	–	–	–
ACProD 3	31.16	48.80	28.45	30.53	20.88	22.96	2.20	2.80	1.26	1.86	–	–	–
ACProD 4	34.64	35.70	30.50	34.04	22.19	25.73	3.45	4.93	0.94	2.92	–	–	–
CProD 1	65.66	55.13	25.67	27.25	17.64	19.22	7.72	8.42	4.57	5.22	–	–	–
CProD 2	60.72	56.64	22.28	22.45	17.27	19.44	5.72	6.02	2.88	3.18	–	–	–
CProD 3	57.98	52.12	24.38	26.14	17.99	20.75	4.46	3.44	1.84	0.82	–	–	–
CProD 4	64.19	60.95	11.20	11.79	19.88	20.47	0	0	0	0	–	–	–

TAProD, AProD, ACProD and CProD refer to tranexamic acid, atenolol, acyclovir and cefuroxime prodrugs, respectively. E_s (INT) is the MM2 calculated strain energy for the tetrahedral intermediate. $\Delta H_f^{\ddagger}$ and $\Delta G_f^{\ddagger}$ are enthalpy and activation energies for the tetrahedral intermediate formation, respectively. $\Delta H_d^{\ddagger}$ and $\Delta G_d^{\ddagger}$ are enthalpy and activation energies for the tetrahedral intermediate dissociation, respectively. k_{rel} (Exp) refers to the experimental relative rate. EM_{exp} and EM_{calc} are the experimental and calculated effective molarities, respectively. H$_2$O and GP refer to calculated in water and the gas phase, respectively
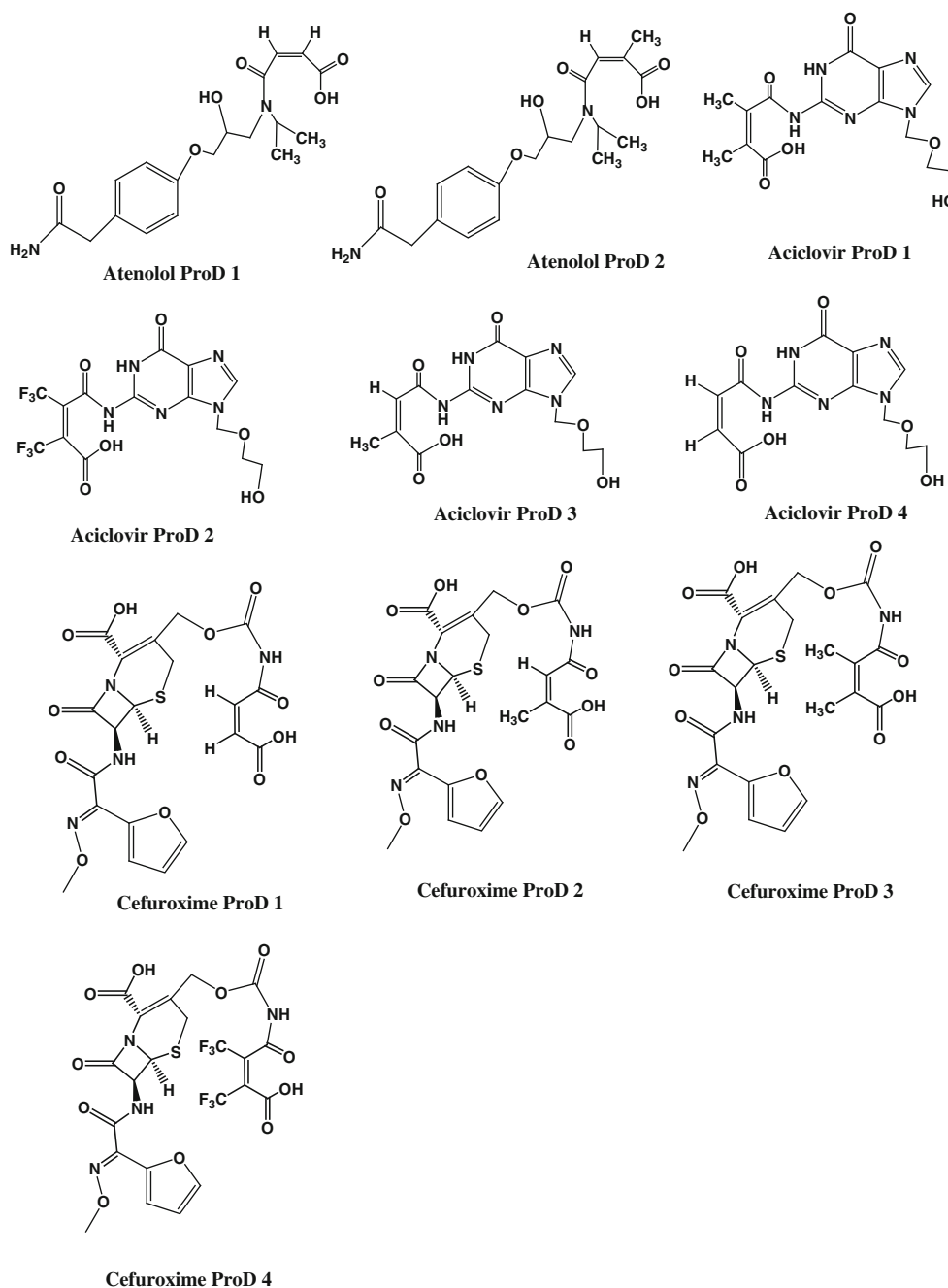
Fig. 6 Chemical structures for atenolol **ProD 1–ProD 2**, acyclovir **ProD 1–ProD 4** and cefuroxime **ProD 1–ProD 4**

the nucleophile to the electrophile barrier; thus the reaction rate will be dependent on the tetrahedral intermediate collapse step (the step via TS_d is the rate-limiting).

For assigning the factor determining the rate-limiting step, the strain energy values for the reactants (GM), and intermediates (INT2) in **1–7** and tranexamic acid prodrugs **ProD 1–ProD 4** were calculated using Allinger's MM2 method [75]. The MM2 calculated strain energies (E_s) values are depicted in Table 2. The E_s values were

correlated with the calculated DFT activation energy values, ($\Delta G_d^{\ddagger}$) (Table 2). Good correlation was obtained between the E_s (INT) in **1–7** and tranexamic acid **ProD 1–ProD 3** and the activation energies for the tetrahedral intermediate breakdown ($\Delta G_d^{\ddagger}$) with a correlation coefficient values r = 0.86 (Fig. 7a). Attempts to correlate the strain energies for the global minimum structures (E_s for GM) with either the experimental log k_{rel} or $\Delta G_d^{\ddagger}$ resulted in a random correlation with r less than 0.40.

Fig. 7 a Plot of activation energy for tetrahedral intermediate dissociation $\Delta G_d^{\ddagger}$ versus strain energy of the tetrahedral intermediate (Es_{INT}) in systems **1–7** and tranexamic acid **ProD 1–ProD 3**. **b** Plot of acid-catalyzed hydrolysis experimental rate (log k_{rel}) versus intermediate strain energy (Es_{INT}) for processes **1–7**. **c** Plot of the DFT calculated effective molarity (EM_{calc}) versus the experimental effective molarity (EM_{exp}) for systems **1–7**
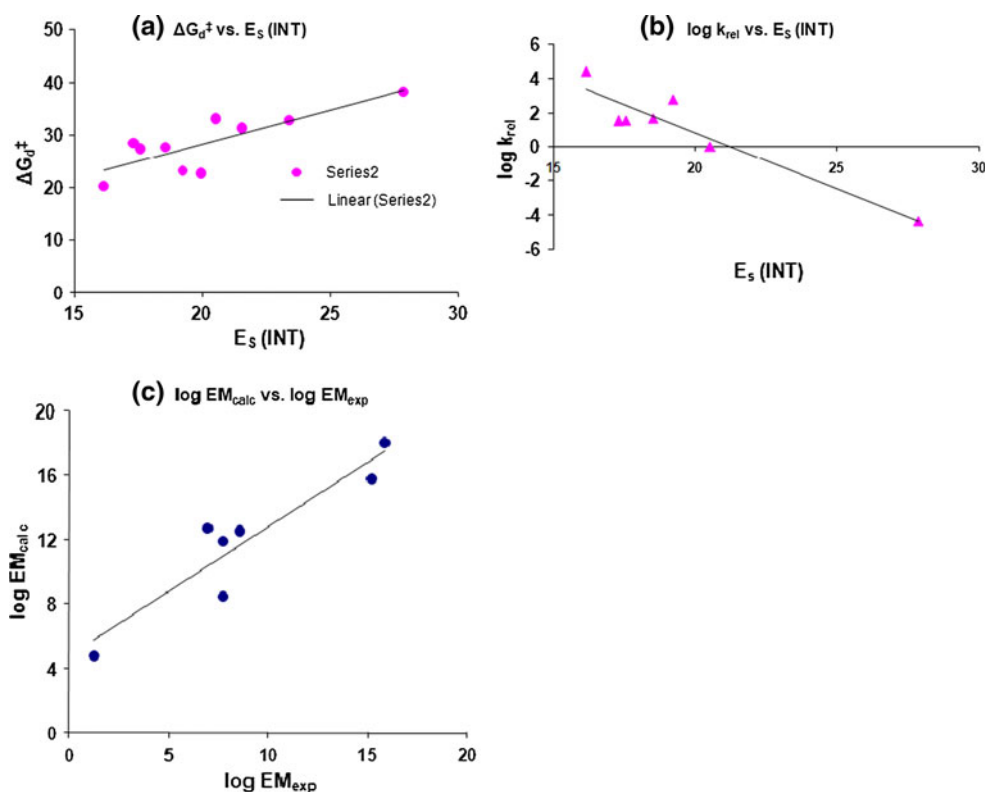
Fig. 8 Schematic representation of the intermolecular process **Inter**

Inter
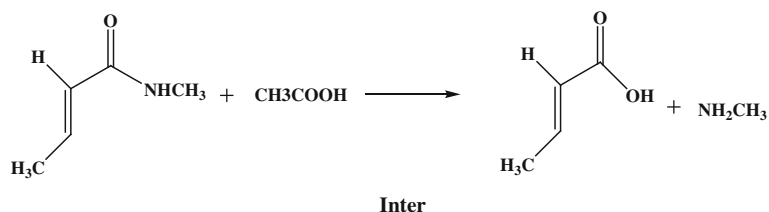
In addition, strong correlation was found between the experimental relative rate (log k_{rel}) and Es (INT) in **1–7** with a correlation coefficient r of 0.95 (Fig. 7b).

Figure 7a, b and Table 2 demonstrate that the reaction rate for systems **1–7** and tranexamic acid **ProD 1–ProD 3** is dependent on the tetrahedral intermediate breakdown and its value is largely affected by the strain energy of the tetrahedral intermediate formed. Systems with less-strained intermediates such as **2** and tranexamic acid **ProD 3** undergo hydrolysis with higher rates than that having more strained intermediates such as **4** and tranexamic acid **ProD 1**. This might be attributed to the fact that the transition state structures in those systems resemble that of the corresponding intermediates.

The effective molarities (EM) for the reactions of **1–7** and tranexamic acid **ProD 1–ProD 4**

The effective molarity parameter is considered an excellent tool to describe the efficiency of a certain intramolecular process. It is generally accepted that the measure for intramolecular efficiency is the effective molarity (EM) which is defined as a ratio of the intramolecular rate (k_{intra}) and its corresponding intermolecular (k_{inter}) where both processes are driven by identical mechanisms. The major factors affecting the EM value are ring size, solvent and reaction type. Values in the order of 10^9–10^{13} M have been measured for the EM in intramolecular processes occurring through nucleophilic addition. Whereas for proton transfer processes EM values of less than 10 M were reported [43] until recently where values of 10^{10} was reported by Kirby on the hydrolysis of some enzyme models [37–41, 43, 76–80].

For obtaining credibility to our calculation results we introduce our computation rational for calculating the EM values for processes **1–7** and tranexamic acid **ProD 1–ProD 4** based on the DFT calculated activation energies ($\Delta G^{\ddagger}$) of **1–7** and tranexamic acid **ProD 1–ProD 4**, and the corresponding intermolecular process **Inter** (Fig. 8).

The intermolecular process **Inter** (Fig. 8) was calculated to be used in the calculation of the effective molarity

values (EM) for the corresponding intramolecular processes **1–7** and tranexamic acid **ProD 1–ProD 4**.

For obtaining the EM values for the reactions of **1–7** and tranexamic acid **ProD 1–ProD 4** we have calculated the kinetic and thermodynamic parameters for their corresponding intermolecular process, **Inter** (Fig. 8).

Using Eqs. 4–7, we have derived Eq. 8 which describes the EM term as a function of the difference in the activation energies of the intra- and the corresponding intermolecular processes. The values calculated using Eq. 8 for processes **1–7** and tranexamic acid **ProD 1–ProD 4** in water are listed in Table 2.

$$EM = k_{intra}/k_{inter} \tag{4}$$

$$\Delta G^{\ddagger}_{inter} = -RT \ln k_{inter} \tag{5}$$

$$\Delta G^{\ddagger}_{intra} = -RT \ln k_{intra} \tag{6}$$

$$\Delta G^{\ddagger}_{intra} - \Delta G^{\ddagger}_{inter} = -RT \ln k_{intra}/k_{inter} \tag{7}$$

$$EM = e^{-(\Delta G^{\ddagger}_{inter} - \Delta G^{\ddagger}_{intra})/RT} \tag{8}$$

where T is 298 °K and R is the gas constant.

The calculated log EM values listed in Table 2 were examined for correlation with the corresponding log EM experimental values [24, 61]. Good correlation was obtained with r value of 0.93 (Fig. 7c). Inspection of the log EM values listed in Table 2 and Fig. 7c reveals that **2**, **5** and tranexamic acid **ProD 3** were the most efficient processes among all processes where by which the tetrahedral intermediate dissociation is the rate-limiting step, whereas processes **1** and **4** were the least. The discrepancy in rates between **2** and **5** on one hand and **1** and **4** on the other hand is attributed to strain effects.

Although the calculated and experimental EM values are comparable there is a discrepancy in their absolute values. This is due to the fact that the experimental measurement of the EM values in **1–7** was conducted in the presence of aqueous acid whereas the DFT calculations were done in water. The dielectric constant value for a mixture of acid/water is expected to be different from that of water (78.39) and hence the discrepancy in the calculated and experimental EM values [24, 69–72].

Calculation of the $t_{1/2}$ values for the cleavage reactions of tranexamic acid prodrugs **ProD 1–ProD 4**

Using Eq. 9 obtained from the correlation of log EM_{calc} versus log EM_{exp} (Fig. 7d) and the $t_{1/2}$ value for process 2 ($t_{1/2} = 1$ s) [61], we have calculated the $t_{1/2}$ values for tranexamic acid **ProD 1–ProD 4**. The predicted $t_{1/2}$ at pH 2 for **ProD 1–ProD 4** as calculated by B3LYP/6-31G(d,p) method are 556, 253 h, 70 s and 1.7 h, respectively.

$$\log EM_{calc} = 0.809 \log EM_{exp} + 4.75 \tag{9}$$

In order to confirm that the DFT calculations at B3LYP/6-31G(d,p) are not dependent on the specific theoretical method used processes **1–3** were calculated at B3LYP/311+G(d,p), hybrid GGA: MPW1k and MP2/6-31G(d,p) levels. The comparisons between the activation energy values calculated by the different methods are listed in Table 3. Careful examination of Table 3 reveals that the calculated values at B3LYP/6-31G(d,p) and B3LYP/311+G(d,p) were very close, whereas, those obtained by either MPW1k [mpwpw91/6-31+G(d,p)] and MP2/6-31G(d,p) were about 2–3 kcal/mol smaller.

Using the calculated energies by the different methods we have calculated the EM values for tranexamic acid **ProD 1** and systems **1–3**. The calculated EM values for tranexamic acid **ProD 1** at B3LYP/6-31G, B3LYP/311+G(d,p) and hybrid GGA: MPW1K [mpwpw91/6-31+G(d,p)] were 9.53, 10.58 and 11.48, respectively. Using the $t_{1/2}$ value for process 2 ($t_{1/2} = 1$ s) [61] and the calculated EM values using the three different methods we have calculated the $t_{1/2}$ values for tranexamic acid **ProD 1** which were 556 h (as calculated by B3LYP/6-31G(d,p), 50.5 h [as calculated by B3LYP/311+G(d,p)] and 6.2 h [as calculated by mpwpw91/6-31+G(d,p)].

Hydrolysis studies

The kinetics of the acid-catalyzed hydrolysis studies were carried out in aqueous buffer in the same manner as that done by Kirby on Kirby's enzyme model **1–7**. This is in order to explore whether the prodrug hydrolyzes in aqueous medium and to what extent or not, suggesting the fate of the prodrug in the system. Acid-catalyzed hydrolysis kinetics of the synthesized tranexamic acid **ProD 1** was studied in four different aqueous media: 1 N HCl, buffer pH 2, buffer pH 5 and buffer pH 7.4. Under the

Table 3 Comparison between calculated energies for **1–3** using B3LYP/6-31G(d,p), B3LYP/6-311+G(d,p), MPW1K and MP2 methods

System	B3L $\Delta H^{\ddagger}_d$	B3L311 $\Delta H^{\ddagger}_d$	MPW1k $\Delta H^{\ddagger}_d$	MP2 $\Delta H^{\ddagger}_d$
1	27.31	27.42	25.07	25.75
2	13.93	14.02	11.96	10.41
3	24.41	23.85	22.61	21.51
ProD 1	28.19	26.76	25.52	–

B3L, B3L311, MPW1k [mpwpw91/6-31+G(d,p)] and MP2 refer to B3LYP/6-31G (d,p), B3LYP/6-311+G(d,p), MPW1K/6-31G(d,p) and MP2/6-31G(d,p) methods, respectively. $\Delta H^{\ddagger}$ is the calculated enthalpy activation energy (kcal/mol). d refers to tetrahedral intermediate dissociation (see Fig. 4). All values were calculated with a molecule of water in the gas phase

Table 4 The observed k value and $t_{1/2}$ of tranexamic acid prodrug (**ProD 1**) In 1 N HCl and at pH 2, 5 and 7.4

| Medium	k_{obs} (h^{-1})	$t_{1/2}$ (h)
1 N HCl	5.13×10^{-3}	0.9
Buffer pH 2	3.92×10^{-5}	23.9
Buffer pH 5	3.92×10^{-6}	270
Buffer pH 7.4	No reaction	No reaction

experimental conditions the target compounds hydrolyzed to release the parent drug (Fig. 6) as evident by HPLC analysis. At constant pH and temperature the reaction displayed strict first order kinetics as the k_{obs} was fairly constant and a straight plot was obtained on plotting log concentration of residual prodrug verves time. The rate constant (k_{obs}) and the corresponding half-lives ($t_{1/2}$) for tranexamic acid prodrug **ProD 1** in the different media were calculated from the linear regression equation correlating the log concentration of the residual prodrug verses time. The kinetic data are listed in Table 4. The 1 N HCl, pH 2 and pH 5 were selected to examine the interconversion of the tranexamic acid prodrug in pH as of stomach, because the mean fasting stomach pH of adult is approximately 1–2 and increases up to 5 following ingestion of food. In addition, buffer pH 5 mimics the beginning small intestine pathway. Finally, pH 7.4 was selected to examine the interconversion of the tested prodrug in blood circulation system. Acid-catalyzed hydrolysis of the tranexamic acid **ProD 1** was found to be higher in 1 N HCl than at pH

2 and 5 (Fig. 9). At 1 N HCl the prodrug was hydrolyzed to release the parent drug in less than 1 h. On the other hand, at pH 7.4, the prodrug was entirely stable and no release of the parent drug was observed. Since the pK_a of tranexamic acid **ProD 1** is in the range of 3–4, it is expected at pH 5 the anionic form of the prodrug will be dominant and the percentage of the free acidic form that undergoes the acid-catalyzed hydrolysis will be relatively low. At 1 N HCl and pH 2 most of the prodrug will exist as the free acid form and at pH 7.4 most of the prodrug will be in the anionic form. Thus, the difference in rates at the different pH buffers.

Conclusions and future directions

The DFT calculations of the acid-catalyzed hydrolysis in Kirby's acid amides **1–7** and tranexamic acid **ProD 1–ProD** revealed that the reaction rate-limiting step depends on the reaction medium. In aqueous medium the rate-limiting step is a dissociation of the tetrahedral intermediate whereas in the gas phase the formation of the tetrahedral intermediate is the rate-limiting step. In addition, the calculations demonstrated that the efficiency of the processes studied is largely sensitive to the pattern of substitution on the carbon–carbon double bond and the nature of the amide N-alkyl group. The reaction rate was found to be linearly correlated with the strain energy of the intermediate (E_s INT). In addition, a linear correlation

Fig. 9 First order hydrolysis plot of tranexamic acid prodrugs **1** in **a** 1 N HCl, **b** buffer of pH 2 and **c** buffer pH 5
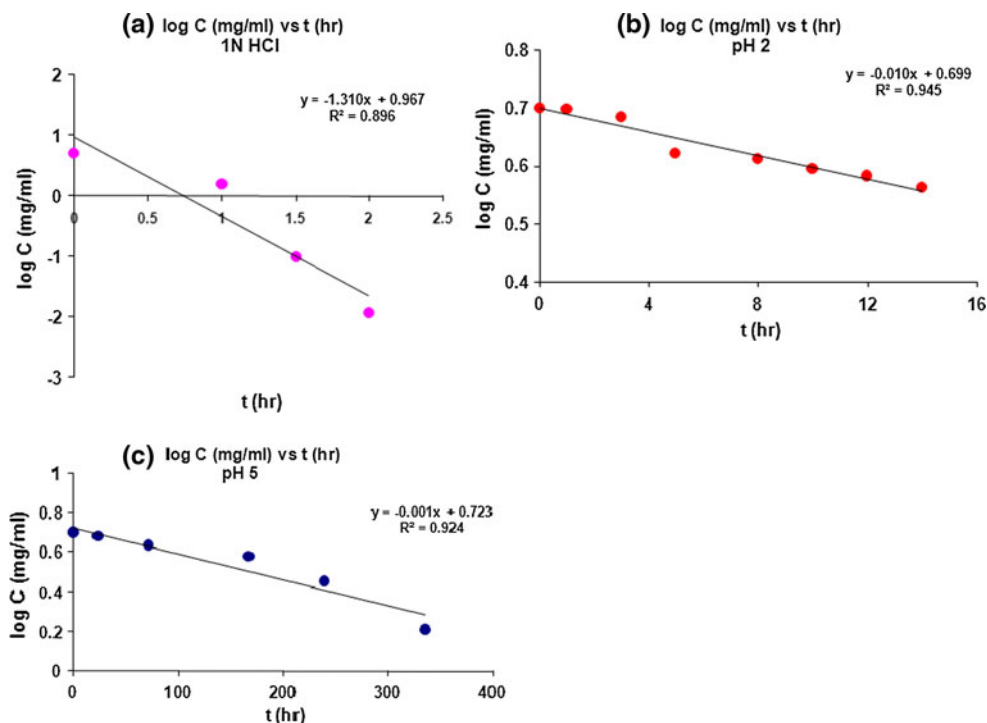
between the calculated and experimental EM values reinforce the credibility of using DFT methods in predicting energies as well as rates for reactions of the type described herein [18–36].

Using the correlation equation obtained from the plot of the calculated and experimental EM values we have calculated the $t_{1/2}$ of four different tranexamic acid prodrugs (**ProD 1**–**ProD 4**).

Comparison between the calculated $t_{1/2}$ values (556 h) for tranexamic acid **ProD 1** to the experimental value (23.9 h) indicates that while the value obtained by B3LYP/6-31G(d,p) is overestimated (about 23 times larger than the experimental) the values obtained by B3LYP/6-311+G(d,p) and mpwpw91/6-31+G(d,p) were much more closer [50.5 h as calculated by B3LYP/311+G(d,p)] and [6.2 h as calculated by mpwpw91/6-31+G(d,p)].

The discrepancy between the calculated B3LYP/6-31G(d,p) and the experimental values might be attributed to (1) B3LYP/6-31G(d,p) is a DFT method without dispersion corrections and (2) PCM solvation model (calculations in presence of solvent) is not capable for handling calculations in acidic aqueous solvent (medium) since the dielectric constant for pH 2 aqueous solutions is not known. In the study calculations the value of 78.39 (dielectric constant for pure water) was used instead.

The $t_{1/2}$ experimental value at pH 5 was 270 h and at pH 7.4 no interconversion was observed. The lack of the reaction at the latter pH might be due to the fact that at this pH tranexamic acid **ProD 1** exists solely in the ionized form (pK_a about 4). As mentioned before the free acid form is a mandatory requirement for the reaction to proceed.

On the other hand, tranexamic acid **ProD 4** has a higher pK_a than tranexamic acid **ProD 1** (about 6 vs. 4). Therefore, it is expected that the interconversion rate of tranexamic acid **ProD 4** to its parent drug, tranexamic acid, at all pHs studied will be higher (log EM for **ProD 4** is 14.33 vs. 9.53 for **ProD 1**).

Future strategy to achieve desirable tranexamic acid prodrugs capable of releasing tranexamic acid in a controlled manner and enhancing the parent drug bioavailability is: (2) synthesis of tranexamic acid **ProD 4**; (2) kinetic studies (in vitro) of **ProD 4** will be performed in at pH 6.5 (intestine) and pH 7.4 (blood circulation system) (3) in vivo pharmacokinetic studies will be done in order to determine the bioavailability and the duration of action of the tested prodrug. Furthermore, based on the in vivo pharmacokinetics characteristics of tranexamic acid **ProD 4** new prodrugs may be design and synthesized.

References

1. Cyklokapron® tranexamic acid injection prescribing information: http://www.pfizer.com/files/products/uspi_cyklokapron.pdf
2. CRASH-2 trial collaborators (2010) Effects of tranexamic acid on death, vascular occlusive events, and blood transfusion in trauma patients with significant haemorrhage (CRASH-2): a randomised, placebo-controlled trial. Lancet 6736(10):60835
3. Gohel M, Patel P, Gupta A, Desai P (2007) Efficacy of tranexamic acid in decreasing blood loss during and after cesarean section: a randomized case controlled prospective study. J Obstet Gynaecol India 57(3):227–230
4. Giancarlo L, Francesco B, Angela L, Pierluigi P, Gina R (2011) Recommendations for the transfusion management of patients in the peri-operative period. II. The intra-operative period. Blood Transfus 9:189–217
5. Lukes AS, Kouides PA, Moore KA (2011) Tranexamic acid: a novel oral formulation for the treatment of heavy menstrual bleeding. Womens Health (Lond Engl) 7(2):151–158
6. Lukes AS, Moore KA, Muse KN, Gersten JK, Hecht BR, Edlund M, Richter HE, Eder SE, Attia GR, Patrick DL, Rubin A, Shangold GA (2010) Tranexamic acid treatment for heavy menstrual bleeding: a randomized controlled trial. Obstet Gynecol 116(4):865–875
7. Ducloy-Bouthors AS, Jude B, Duhamel A, Broisin F, Huissoud C, Keita-Meyer H, Mandelbrot L, Tillouche N, Fontaine S, Le Goueff F, Depret-Mosser S, Vallet B, EXADELI Study Group, Susen S (2011) High-dose tranexamic acid reduces blood loss in postpartum haemorrhage. Crit Care 15(2):R117. doi:10.1186/cc10143 (Epub 2011 Apr 15)
8. Ayedi M, Jarraya A, Smaoui M, Zouari J, Smaoui L, Kolsi K (2011) Effect of tranexamic acid on post partum hemorrhage by uterine atony: a preliminary result of a randomized, placebo-controlled trial: 11AP4-7. Eur J Anaesthesiol 28:165
9. Gungorduk K, Yıldırım G, Asıcıoğlu O, Gungorduk OC, Sudolmus S, Ark C (2011) Efficacy of intravenous tranexamic acid in reducing blood loss after elective cesarean section: a prospective, randomized, double-blind, placebo-controlled study. Am J Perinatol 28(3):233–240
10. Sekhavat L, Tabatabaii A, Dalili M, Farajkhoda T, Tafti AD (2009) Efficacy of tranexamic acid in reducing blood loss after cesarean section. J Matern Fetal Neonatal Med 22(1):72–75
11. Sentürk MB, Cakmak Y, Yildiz G, Yildiz P (2012) Tranexamic acid for cesarean section: a double-blind, placebo-controlled, randomized clinical trial. Arch Gynecol Obstet. Nov 11 [Epub ahead of print]
12. Cardone D, Klein AA (2009) Perioperative blood conservation. Eur J Anaesthesiol 26:722–729
13. Nilsson IM (1980) Clinical pharmacology of aminocaproic and tranexamic acids. J Clin Pathol 33(14):41–47
14. Turki A, Michael W (2011) Tranexamic acid treatment of life-threatening hematuria in polycystic kidney disease (case report). Int J Nephrol 2011:203579. doi:10.4061/2011/203579
15. Maedaa K, Naganuma M (1998) Topical trans-4-aminomethyl cyclohexane carboxylic acid prevents ultraviolet radiation-induced pigmentation. J Photochem Photobiol B 47:136–141
16. Sufan W, Hangyan S, Hua W, Sheng Y, Jincai G, Yi S, Lei P (2012) Treatment of melasma with oral administration of tranexamic acid. Aesthet Plast Surg 36:964–970

17. Pilbrant A, Schannong M, Vessman J (1981) Pharmacokinetics and bioavailability of tranexamic acid. Eur J Clin Pharmacol 20(1):65–72

18. Karaman R (2008) Analysis of Menger's spatiotemporal hypothesis. Tetrahedron Lett 49:5998–6002

19. Karaman R (2009) Cleavage of Menger's aliphatic amide: a model for peptidase enzyme solely explained by proximity orientation in intramolecular proton transfer. J Mol Struct (Theochem) 910:27–33

20. Karaman R (2010) The efficiency of proton transfer in Kirby's enzyme model, a computational approach. Tetrahedron Lett 51:2130–2135

21. Karaman R, Pascal RA (2010) Computational analysis of intramolecularity in proton transfer reactions. Org Biomol Chem 8:5174–5178

22. Karaman R (2010) A general equation correlating intramolecular rates with 'attack' parameters: distance and angle. Tetrahedron Lett 51:5185–5190

23. Karaman R (2011) Analyzing the efficiency of proton transfer to carbon in Kirby's enzyme model—a computational approach. Tetrahedron Lett 52:699–704

24. Karaman R (2011) Analyzing the efficiency in intramolecular amide hydrolysis of Kirby's N-alkylmaleamic acids—a computational approach. Comput Theor Chem 974:133–142

25. Karaman R (2009) A new mathematical equation relating activation energy to bond angle and distance: a key for understanding the role of acceleration in lactonization of the trimethyl lock system. Bioorg Chem 37:11–25

26. Karaman R (2009) Revaluation of Bruice's proximity orientation. Tetrahedron Lett 50:452–458

27. Karaman R (2009) Accelerations in the lactonization of trimethyl lock systems are due to proximity orientation and not to strain effects. Res Lett Org Chem. doi:10.1155/2009/240253

28. Karaman R (2009) The gem-disubstituent effect—a computational study that exposes the relevance of existing theoretical models. Tetrahedron Lett 50:6083–6087

29. Karaman R (2009) Analyzing Kirby's amine olefin—a model for amino-acid ammonia lyases. Tetrahedron Lett 50:7304–7309

30. Karaman R (2009) The effective molarity (EM) puzzle in proton transfer reactions. Bioorg Chem 37:106–110

31. Karaman R (2010) Effects of substitution on the effective molarity (EM) for five membered ring-closure reactions—a computational approach. J Mol Struct (Theochem) 939:69–74

32. Karaman R (2010) The effective molarity (EM) puzzle in intramolecular ring-closing reactions. J Mol Struct (Theochem) 940:70–75

33. Menger FM, Karaman R (2010) A singularity model for chemical reactivity. Eur J Chem 16:1420–1427

34. Karaman R (2010) The effective molarity (EM)—a computational approach. Bioorg Chem 38:165–172

35. Karaman R (2010) Proximity vs. strain in ring-closing reactions of bifunctional chain molecules—a computational approach. J Mol Phys 108:1723–1730

36. Karaman R (2011) The role of proximity orientation in intramolecular proton transfer reactions. J Comput Theor Chem 966:311–321

37. Barber SE, Dean KES, Kirby AJ (1999) A mechanism for efficient proton-transfer catalysis. Intramolecular general acid catalysis of the hydrolysis of 1-arylethyl ethers of salicylic acid. Can J Chem 77:792–801

38. Kirby AJ, de Silva MF, Lima D, Roussev CD, Nome F (2006) Efficient intramolecular general acid catalysis of nucleophilic attack on a phosphodiester. J Am Chem Soc 128:16944–16952

39. Kirby AJ, Williams NH (1994) Efficient intramolecular general acid catalysis of enol ether hydrolysis. Hydrogen-bonding stabilization of the transition state for proton transfer to carbon. J Chem Soc Perkin Trans 2:643–648

40. Kirby AJ, Williams NH (1991) Efficient intramolecular general acid catalysis of vinyl ether hydrolysis by the neighbouring carboxylic acid group. J Chem Soc Chem Commun 1643–1644

41. Kirby AJ (1996) Enzyme mechanisms, models, and mimics. Angew Chem Int Ed Engl 35:706–724

42. Fife TH, Przystas TJ (1979) Intramolecular general acid catalysis in the hydrolysis of acetals with aliphatic alcohol leaving groups. J Am Chem Soc 101:1202–1210

43. Kirby AJ (2005) Effective molarities for intramolecular reactions. J Phys Org Chem 18:101–278

44. Menger FM, Ladika M (1988) Fast hydrolysis of an aliphatic amide at neutral pH and ambient temperature. A peptidase model. J Am Chem Soc 110:6794–6796

45. Menger FM (1985) On the source of intramolecular and enzymatic reactivity. Acc Chem Res 18:128–134

46. Menger FM, Chow JF, Kaiserman H, Vasquez PC (1983) Directionality of proton transfer in solution. Three systems of known angularity. J Am Chem Soc 105:4996–5002

47. Menger FM, Galloway AL, Musaev DG (2003) Relationship between rate and distance. Chem Commun 2370–2371

48. Milstein S, Cohen LA (1970) Concurrent general-acid and general-base catalysis of esterification. J Am Chem Soc 92:4377–4382

49. Milstein S, Cohen LA (1970) Rate acceleration by stereopopulation control: models for enzyme action. Proc Natl Acad Sci USA 67:1143–1147

50. Milstein S, Cohen LA (1972) Stereopopulation control I. Rate enhancement in the lactonizations of o-hydroxyhydrocinnamic acids. J Am Chem Soc 94:9158–9165

51. Brown RF, van Gulick NM (1956) The geminal alkyl effect on the rates of ring closure of bromobutylamines. J Org Chem 21:1046–1049

52. Bruice TC, Pandit UK (1960) The effect of geminal substitution ring size and rotamer distribution on the intra molecular nucleophilic catalysis of the hydrolysis of monophenyl esters of dibasic acids and the solvolysis of the intermediate anhydrides. J Am Chem Soc 82:5858–5865

53. Bruice TC, Pandit UK (1960) Intramolecular models depicting the kinetic importance of ''Fit'' in enzymatic catalysis. Proc Natl Acad Sci USA 46:402–404

54. Galli C, Mandolini L (2000) The role of ring strain on the ease of ring closure of bifunctional chain molecules. Eur J Org Chem 2000:3117–3125

55. Karaman R (2010) Prodrugs of aza nucleosides based on proton transfer reactions. J Comput Aided Mol Des 24:961–970

56. Karaman R (2011) Computational aided design for dopamine prodrugs based on novel chemical approach. Chem Biol Drug Des 78:853–863

57. Karaman R, Dajani KK, Qtait A, Khamis M (2012) Prodrugs of acyclovir—a computational approach. Chem Biol Drug Des 79:819–834

58. Karaman R, Hallak H (2010) Computer-assisted design of prodrugs for antimalarial atovaquone. Chem Biol Drug Des 76:350–360

59. Karaman R, Dajani KK, Hallak H (2012) Computer-assisted design for atenolol prodrugs for the use in aqueous formulations. J Mol Model 18:1523–1540

60. Hejaz H, Karaman R, Khamis M (2012) Computer-assisted design for paracetamol masking bitter taste prodrugs. J Mol Model 18:103–114

61. Kirby AJ, Lancaster PW (1972) Structure and efficiency in intramolecular and enzymatic catalysis. Catalysis of amide hydrolysis by the carboxy-group of substituted maleamic acids. J Chem Soc Perkin Trans 2:1206–1214

62. Zhao Y, Truhlar DG (2008) Density functionals with broad applicability in chemistry. Acc Chem Res 41(2):157–167

63. Zhao Y, Truhlar DG (2008) Exploring the limit of accuracy of the global hybrid meta density functional for main-group thermo-chemistry, kinetics, and noncovalent interactions.". J Chem Theory Comput 4(11):1849–1868

64. Zheng J, Zhao Y, Truhlar DG (2009) The DBH24/08 database and its use to assess electronic structure model chemistries for chemical reaction barrier heights. J Chem Theory Comput 5(4):808–821

65. Gaussian 09, Revision **A.1**, Frisch MJ, Trucks GW, Schlegel HB, Scuseria GE, Robb MA, Cheeseman JR, Scalmani G, Barone V, Mennucci B, Petersson GA, Nakatsuji H, Caricato M, Li X, Hratchian HP, Izmaylov AF, Bloino J, Zheng G, Sonnenberg JL, Hada M, Ehara M, Toyota K, Fukuda R, Hasegawa J, Ishida M, Nakajima T, Honda Y, Kitao O, Nakai H, Vreven T, Montgomery Jr JA, Peralta JE, Ogliaro F, Bearpark M, Heyd JJ, Brothers E, Kudin K. N, Staroverov V. N, Kobayashi R, Normand J, Ragh-avachari K, Rendell A, Burant J. C, Iyengar S. S, Tomasi J, Cossi M, Rega N, Millam JM, Klene M, Knox JE, Cross JB, Bakken V, Adamo C, Jaramillo J, Gomperts R, Stratmann RE, Yazyev O, Austin AJ, Cammi R, Pomelli C, Ochterski JW, Martin RL, Morokuma K, Zakrzewski VG, Voth GA, Salvador P, Dannen-berg JJ, Dapprich S, Daniels AD, Farkas Ö, Foresman JB, Ortiz JV, Cioslowski J, Fox DJ (2009) Gaussian, Inc., Wallingford CT

66. Casewit CJ, Colwell KS, Rappe' AK (1992) Application of a universal force field to main group compounds. J Am Chem Soc 114:10046–10053

67. Murrell JN, Laidler KJ (1968) Symmetries of activated com-plexes. Trans Faraday Soc 64:371–377

68. Muller K (1980) Reaction paths on multidimensional energy hypersurfaces. Angew Chem Int Ed Engl 19:1–13

69. Cancès MT, Mennucci B, Tomasi J (1997) A new integral equation formalism for the polarizable continuum model: theo-retical background and applications to isotropic and anisotropic dielectrics. J Chem Phys 107:3032–3041

70. Mennucci B, Tomasi J (1997) Coninuum solvation models: a new approach to the problem of solute's charge distribution and cavity boundaries. J Chem Phys 106:5151

71. Mennucci B, Cancès MT, Tomasi J (1997) Evaluation of solvent effects in isotropic and anisotropic dielectrics and in ionic solu-tions with a unified integral equation method: theoretical bases, computational implementation, and numerical applications. J Phys Chem B 101:10506–10517

72. Tomasi J, Mennucci B, Cancès MT (1997) The IEF version of the PCM solvation method: an overview of a new method addressed to study molecular solutes at the QM ab initio level. J Mol Struct (Theochem) 464:211–226

73. Kluger R, Chin J (1982) Carboxylic acid participation in amide hydrolysis. Evidence that separation of a nonbonded complex can be rate determining. J Am Chem Soc 104:2891–2897

74. Katagi T (1990) AM1 study of acid-catalyzed hydrolysis of maleamic (4-amino-4-oxo-2-butenoic) acids. J Comput Chem 11(9):1094–1100

75. Burker U, Allinger NL (1982) Molecular mechanics. American Chemical Society, Washington, DC

76. Kirby AJ, Parkinson A (1994) Most efficient intramolecular general acid catalysis of acetal hydrolysis by the carboxyl group. J Chem Soc Chem Commun 707–708

77. Brown CJ, Kirby AJ (1997) Efficiency of proton transfer catal-ysis. Intramolecular general acid catalysis of the hydrolysis of dialkyl acetals of benzaldehyde. J Chem Soc Perkin Trans 2:1081–1094

78. Craze G-A, Kirby AJ (1974) The role of the carboxy-group in intramolecular catalysis of acetal hydrolysis. The hydrolysis of substituted 2- methoxymethoxybenzoic acids. J Chem Soc Perkin Trans 2:61–66

79. Hartwell E, Hodgson DRW, Kirby AJ (2000) Exploring the limits of efficiency of proton-transfer catalysis in models and enzymes. J Am Chem Soc 122:9326–9327

80. Kirby AJ (1997) Efficiency of proton transfer catalysis in models and enzymes. Acc Chem Res 30:290–296